Applied Mathematical Modelling 39 (2015) 600–620

Contents lists available at ScienceDirect

Applied Mathematical Modelling

journal homepage: www.elsevier.com/locate/apm

Vibration absorber design to suppress regenerative chatter in nonlinear milling process: Application for machining of cantilever plates

Hamed Moradi *, Gholamreza Vossoughi [1], Mehdi Behzad [1], Mohammad R. Movahhedy [1]

Centre of Excellence in Design, Robotics and Automation (CEDRA), School of Mechanical Engineering, Sharif University of Technology, Tehran, Iran

ARTICLE INFO

Article history:
Received 16 November 2012
Received in revised form 12 April 2014
Accepted 19 June 2014
Available online 1 July 2014

Keywords:
Tunable vibration absorber
Milling process
Cantilever plate
Nonlinear model
Chatter suppression

ABSTRACT

In this paper, a tunable vibration absorber (TVA) is designed to suppress regenerative chatter in milling of cantilever plates. In machining industry, the majority of work-piece materials or the interaction of work-piece/cutting tool causes the cutting forces to demonstrate nonlinear behavior. The application of TVA (as a semi-active controller) is investigated for the process with an extensive nonlinear model of cutting forces. Under regenerative chatter conditions, optimum values of the absorber position and its spring stiffness are found such that the plate vibration is minimized. For this purpose, an optimal algorithm is developed based on mode summation approach. Results are presented and compared for two cases: regenerative chatter under resonance and non-resonance conditions. It is shown that the absorber acts efficiently in chatter suppression of both machining conditions, in a wide range of chatter frequencies. Moreover, using TVA leads to the great improvement in stability limits of the process. Therefore, larger values of depth of cut and consequently more material removal rate can be obtained without moving to the unstable machining conditions.

1. Introduction

One of the major machining processes is the peripheral milling. It is especially implemented in aerospace industries where the end mills are used for milling of wing parts and engine components. However, its appropriate performance may be unreachable due to existence of various types of vibrations. In machining processes, self-excited vibration or chatter is the most important type of vibration. Reduction of tool life, poor surface quality and decrease in productivity rate are the adverse affects of chatter vibrations.

Machine tool chatter is caused either by regeneration or mode coupling, as two well known mechanisms. In machining processes, the regenerative type is found to be the most important mode of chatter vibration. It occurs when the cut produced at time t leaves a wavy surface on the material regenerated during subsequent passes of cut (Fig. 1). The phase difference between the inner and outer waves and the dynamic gain of the system play a key role in stability of the cutting process. In second mechanism, when there is no interaction between the vibration of the system and undulated surface of

* Corresponding author. Tel.: +98 21 66165545; fax: +98 21 66000021.
E-mail addresses: hamedmoradi@mech.sharif.ir, hamedmoradi@asme.org (H. Moradi).
[1] Tel.: +98 21 66165694; fax: +98 21 66000021.

http://dx.doi.org/10.1016/j.apm.2014.06.010
0307-904X/

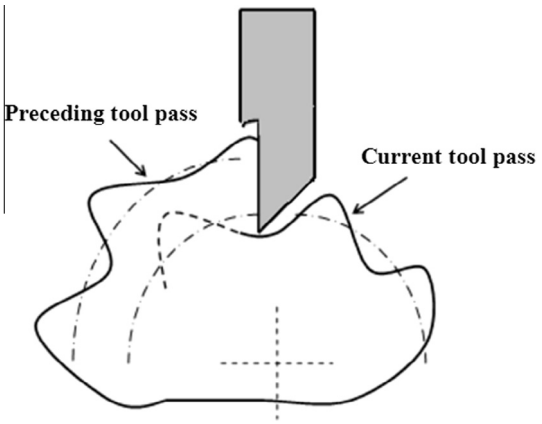

Fig. 1. Chatter instability caused by the regeneration mechanism.

the work-piece, usually mode coupling occurs. Consequently, the tool traces out an elliptic path that varies the depth of cut in such a way as to intensify the coupled modes of vibrations [1].

For the purpose of chatter prediction in high speed and high precision cutting processes, accurate models are required. To obtain dynamic equations of various milling processes and prediction of cutting forces, deflection of machine components and form errors, mechanistic approach has been extensively used [2,3]. In milling process, when the cutter has a uniform pitch, the cutting forces are periodic at tooth passing intervals (due to multiple teeth cutter).

In milling process, chatter stability has been investigated in the frequency and discrete time domains for the linear models. Also, analytical solutions have been developed for direct prediction of stability lobes in the frequency domain [4] and prediction of stability limits in high-speed milling (while multi-mode dynamics is considered) [5]. In discrete time domain and for stability analysis, various methods have been used for direct inclusion of periodically varying system parameters. Time finite element analysis (TFEA) to investigate limit cycles and bifurcation behavior [6]; semi-discretization and full-discretization methods (SDM & FDM) for determination of stability lobes diagram [7–12]; and TFEA for simultaneous predictions of stability and surface location error have been used [13].

In addition, SDM and TFEA have been used in analytical prediction of chatter stability for variable pitch and variable helix tools [14]. Also, TEFA and Chebyshev collocation methods based on harmonic balance approach have been applied for stability analysis [15]. A comparison between frequency and semi-discrete time solutions of the chatter stability [16]; and a fuzzy stability analysis for different domains have been presented [17].

Due to recent machining of materials with severe nonlinear characteristics, nonlinear modeling of the chatter phenomenon has received more attention. Considering the square and cubic polynomial terms related to the cutting forces, structural stiffness and power-law functions for cutting forces, delayed nonlinear models of the process have been governed [18–21]. Also, other sources of nonlinearity in machining processes have been recognized including the visco-elastic and hysteresis effects, variable friction, thermo-mechanical effect and intermittent engagement of the cutting tool [22].

In the previous researches [23,24], the extended nonlinear modeling of cutting forces and development of closed form expression through Fourier series expansion have been accomplished. Considering the structural and cutting forces nonlinearities, dynamics of regenerative chatter and internal resonance phenomenon was investigated [23]. In other research, nonlinear dynamics and bifurcation analysis of the milling process in the presence of tool wear, process damping and cutting force nonlinearities was studied [24].

To suppress regenerative chatter in machining processes, various passive and active control approaches have been used. Tunable vibration absorbers and tuned viscoelastic dampers for turning [25,26], boring [27,28] and milling processes have been used as some effective passive techniques [29,30]. Also, for the case of nonlinear cutting forces in milling operations, a tunable vibration absorber was designed to suppress regenerative chatter and improve stability limits of the process [12].

It should be mentioned that in the previous work [12], tunable vibration absorbers (TVAs) were designed to suppress regenerative chatter of the milling process in which the cutting tool was modeled as an Euler–Bernoulli beam (as a continuous vibrating system). That case essentially occurs when a relatively long extension part is used (in milling processes where the access to the work-piece is difficult due to work-space limitations). In [12], the work-piece dynamics was assumed to be rigid and all the structure flexibility was considered in the cutting tool. In this research (unlike [12]), the cutting tool is modeled as a lumped rigid 2DOF model (due to its short length), while all the structural flexibility is considered in the thin plate work-piece. Therefore, the scope of current research is completely different from the previous [12], both in physical implementation and engineering applications.

Moreover, to avoid chatter vibrations, the changing and selection of spindle speed have been studied [31–34]. In the category of active vibration control, various works have been developed such as active vibration absorbers [35] and model reference adaptive control to achieve constant cutting forces, e.g., [34,36]. In addition, active control systems for chatter

suppression [37,38] have been implemented and sliding mode control and robust control of regenerative chatter have been proposed [39,40].

However in the majority of previous works, control strategies have been implemented in which the cutting tool or the work-piece is considered as a one/two degrees of freedom model (SDOF/2DOF). During the milling process of plates, for the cases where a cutting tool with relatively short extension part is used, this assumption may not be adequately accurate. Although the short cutting tool (with very high natural frequencies) can be considered as a rigid body, plate work-piece is a continuous system and contains infinite number of vibration modes. Therefore, if only the dominant mode is considered in construction of control strategy, the rest of the structural modes may be excited; leading to the undesirable vibrations.

In this paper, a tunable vibration absorber (TVA) is designed for chatter suppression in the milling of plate work-pieces, with nonlinear cutting force characteristics. Unlike the previous research [12] in which the cutting tool and work-piece were modeled as flexible and rigid body parts (respectively), the short cutting tool is assumed to be rigid while the plate work-piece is the flexible component. Unlike the previous work [41], where TVA was designed for a cantilever plate under the simple harmonic excitation (not in machining), closed form expressions for the nonlinear cutting forces are considered here.

In the presence of nonlinear regenerative chatter with associated time delay terms, the extensive formulation of the process including the plate and attached absorber is presented. Developing an algorithm based on mode summation technique, optimum values of the absorber position and its spring stiffness are found such that the plate vibration is minimized. Simulation results are presented and compared for two cases: regenerative chatter under resonance and non-resonance conditions. For both machining conditions and in a wide range of chatter frequencies, TVA acts efficiently in chatter suppression. It also improves the stability limits of process. Therefore, larger values of depth of cut and consequently more material removal rate can be obtained, while dynamic system is stable.

2. Dynamics of the peripheral milling process in the presence of nonlinear regenerative chatter

2.1. Classical linear model of the cutting forces

Dynamics of the cutting forces in peripheral milling process is shown in Fig. 2. The immersion angle is measured clockwise from the y-axis and the axial (a_c) and radial (w) depths of cut are constant. Assuming the bottom end of one flute as the reference immersion angle ϕ, the bottom end points of other flutes are described at the angles:

$$\phi_j(0) = \phi + j\phi_p; \quad j = 0, 1, \ldots, (N-1); \quad \phi_p = 2\pi/N, \tag{1}$$

where ϕ_p is the cutter pitch angle and N is the number of cutter teeth. Considering the lag angle at an arbitrary axial depth of cut z, the immersion angle of flute j is expressed as [42]:

$$\phi_j(z) = \phi + j\phi_p - (2z/D)\tan\beta; \quad j = 0, 1, \ldots, (N-1), \tag{2}$$

where β and D are helix angle and diameter of the cutter, respectively. Considering the cutting coefficients contributed by the shearing and edge actions in tangential ($K_{tc},\ K_{te}$) and radial ($K_{rc},\ K_{re}$) directions (while in 2D modeling, cutting force in the axial direction is assumed to be negligible with respect to other components), acting cutting forces on a differential flute element with height dz are expressed as:

$$\begin{aligned} \mathrm{d}F_{t,j}(\phi, z) &= [K_{tc}\, h_j(\phi_j(z)) + K_{te}]\, \mathrm{d}z, \\ \mathrm{d}F_{r,j}(\phi, z) &= [K_{rc}\, h_j(\phi_j(z)) + K_{re}]\, \mathrm{d}z, \end{aligned} \tag{3}$$

where the chip thickness is:

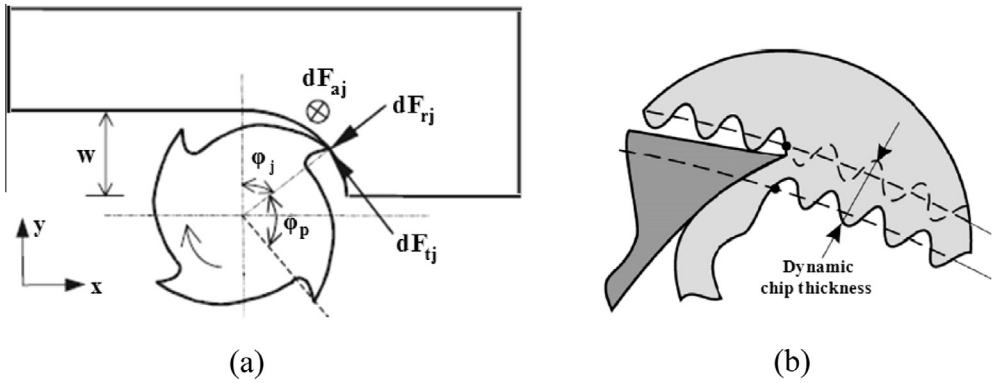

Fig. 2. (a) Cutting forces in the peripheral milling process (b) dynamic chip thickness in regenerative chatter (Source: [16,42]).

$$h_j(\phi,z) = c_f \sin\phi_j(z) \tag{4}$$

and c_f is the feed per revolution. According to coordinates shown in Fig. 2, elemental forces in feed (x) and normal (y) directions are expressed in terms of tangential and radial forces as:

$$\begin{aligned} dF_{x,j}(\phi,z) &= -dF_{t,j}\cos\phi_j(z) - dF_{r,j}\sin\phi_j(z),\\ dF_{y,j}(\phi,z) &= +dF_{t,j}\sin\phi_j(z) - dF_{r,j}\cos\phi_j(z). \end{aligned} \tag{5}$$

Substituting Eqs. (3) and (4) in Eq. (5) and integrating analytically along the cut portion of the flute j, yields the closed form expressions for cutting forces (see [42] for more details). The cutting forces contributed by all flutes are integrated digitally to obtain the total forces as:

$$F_x(\phi) = \sum_{j=0}^{N-1} F_{xj}; \quad F_y(\phi) = \sum_{j=0}^{N-1} F_{yj}. \tag{6}$$

2.2. Cutting forces in the presence of nonlinear regenerative chatter

Under machining conditions where cutting forces are inherently nonlinear functions of dynamic chip thickness (e.g., Titanium alloys), nonlinear modeling of the process is essential [18–24,42,43]. In addition, stability theories based on linear dynamics cannot predict stability limits in correlation with those of obtained experimentally. Nonlinear modeling of cutting forces is arisen from nonlinear material constitutive relations [20–22]. To achieve a more realistic model, cutting forces are expressed as a complete third-order polynomial function of cut chip thickness as [12,23,24]:

$$\begin{aligned} dF_{t,j}(\phi,z) &= [\xi_1 h_j^3(\phi_j(z)) + \xi_2 h_j^2(\phi_j(z)) + \xi_3 h_j(\phi_j(z)) + \xi_4]\,dz,\\ dF_{r,j}(\phi,z) &= [\delta_1 h_j^3(\phi_j(z)) + \delta_2 h_j^2(\phi_j(z)) + \delta_3 h_j(\phi_j(z)) + \delta_4]\,dz, \end{aligned} \tag{7}$$

where cutting force coefficients $\xi_i,\ \delta_i,\ i = 1,\ldots,4$ are found directly from experimental force signals. The input excitations are the cutting force components in tangential and radial directions (or consequently, F_x and F_y in x–y directions). These cutting force components can be measured by a dynamometer in the absence/presence of regenerative chatter. After cutting force measurements, their components F_t and F_r are plotted versus chip thickness h. Then, using the linear regression via Curve Fitting Toolbox of MATLAB, applied on Eq. (7) in un-differential form, cutting force coefficients, $\xi_i,\ \delta_i,\ i = 1,\ldots,4$ can be obtained. Details of this identification procedure, implemented on some experimental cutting force data, have been presented in [23,43].

It should be mentioned that the proposed nonlinear model of cutting forces (Eq. (7)) has an acceptable accuracy for a relatively wide range of chip thicknesses. This is because, a complete third-order polynomial function is considered for cutting forces as functions of chip thickness (unlike the previous researches [18–22,42], where a power-law function for cutting forces was considered and then approximated through Taylor series). Especially, the efficiency of proposed nonlinear modeling is more obvious when we deal with the machining conditions where cutting forces are inherently nonlinear functions of dynamic chip thickness (e.g., machining of Titanium alloys) [18,20–22,42]. In the presence of regenerative chatter, the variable total chip thickness is expressed as (instead of Eq. (4)):

$$h(\phi_j) = [c_f \sin\phi_j + v_{j,0} - v_j]\,g(\phi_j), \tag{8}$$

where c_f is the feed per tooth per revolution; $c_f \sin\phi_j$ is the static part of the chip thickness caused by rigid body motion of the cutter and $v_{j,0} - v_j$ is the dynamic part; produced due to vibrations of the tool at the present (v_j) and previous ($v_{j,0}$) tooth periods. $g(\phi_j)$ is a unit step function determining whether the tooth is in or out of cut and is described in terms of start (ϕ_{st}) and exit immersion (ϕ_{ex}) angles of the cutter as:

$$g(\phi_j) = \begin{cases} 1 & \phi_{st} < \phi_j < \phi_{ex},\\ 0 & \phi_{st} > \phi_j \text{ or } \phi_{ex} < \phi_j. \end{cases} \tag{9}$$

Since the static part of chip thickness ($c_f \sin\phi_j$) has no effect on the dynamic chip load regeneration mechanism, e.g., [1,4,6–16], and according to the coordinates shown in Fig. 2, Eq. (8) is reduced to:

$$h(\phi_j) = [\Delta x \sin\phi_j + \Delta y \cos\phi_j]\,g(\phi_j), \tag{10}$$

where

$$\Delta x = x(t) - x(t-\tau); \quad \Delta y = y(t) - y(t-\tau); \quad \tau = 2\pi/(N\Omega), \tag{11}$$

$[x(t),y(t)]$ and $[x(t-\tau),y(t-\tau)]$ represent dynamic displacements of the cutter at the present and previous tooth periods and τ is the delay time; where Ω (rad/s) is the spindle speed.

In the previous researches [12,23,24], the extended nonlinear modeling of cutting forces and development of closed form expression through Fourier series expansion have been accomplished. According to the formulation presented there, closed form expressions for nonlinear cutting forces in x–y directions are explained as:

$$F_x = -\frac{N}{2\pi}\{\alpha_1\Delta x^3 + \beta_1\Delta y^3 + \alpha_2\Delta x^2 + \beta_2\Delta y^2 + \alpha_3\Delta x + \beta_3\Delta y + 3\gamma_1\Delta x^2\Delta y + 3\gamma_2\Delta x\Delta y^2 + 2\gamma_3\Delta x\Delta y + \gamma_4\},$$
$$F_y = +\frac{N}{2\pi}\{\alpha'_1\Delta x^3 + \beta'_1\Delta y^3 + \alpha'_2\Delta x^2 + \beta'_2\Delta y^2 + \alpha'_3\Delta x + \beta'_3\Delta y + 3\gamma'_1\Delta x^2\Delta y + 3\gamma'_2\Delta x\Delta y^2 + 2\gamma'_3\Delta x\Delta y + \gamma'_4\}, \tag{12}$$

where for the half immersion up-milling with $\phi_{st} = 0$ and $\phi_{ex} = \pi/2$ (as for the case study here), coefficients of Eq. (12) are determined in terms of $\xi_i,\ \delta_i\ i = 1,\ldots,4$ as:

$$\alpha_1 = \frac{1}{4}\left[\xi_1 + \frac{3}{4}\pi\delta_1\right] \quad \beta_1 = \frac{1}{4}\left[\delta_1 + \frac{3}{4}\pi\xi_1\right] \quad \alpha_2 = \frac{1}{3}[\xi_2 + 2\delta_2] \quad \beta_2 = \frac{1}{3}[\delta_2 + 2\xi_2] \quad \alpha_3 = \frac{1}{2}\left[\xi_3 + \frac{1}{2}\pi\delta_3\right],$$
$$\beta_3 = \frac{1}{2}\left[\delta_3 + \frac{1}{2}\pi\xi_3\right] \quad \gamma_1 = \frac{1}{4}\left[\delta_1 + \frac{1}{4}\pi\xi_1\right] \quad \gamma_2 = \frac{1}{4}\left[\xi_1 + \frac{1}{4}\pi\delta_1\right] \quad \gamma_3 = \frac{1}{3}[\delta_2 + \xi_2] \quad \gamma_4 = \xi_4 + \delta_4,$$
$$\alpha'_1 = \frac{1}{4}\left[-\delta_1 + \frac{3}{4}\pi\xi_1\right] \quad \beta'_1 = \frac{1}{4}\left[\xi_1 - \frac{3}{4}\pi\delta_1\right] \quad \alpha'_2 = \frac{1}{3}[-\delta_2 + 2\xi_2] \quad \beta'_2 = \frac{1}{3}[\xi_2 - 2\delta_2] \quad \alpha'_3 = \frac{1}{2}\left[-\delta_3 + \frac{1}{2}\pi\xi_3\right],$$
$$\beta'_3 = \frac{1}{2}\left[\xi_3 - \frac{1}{2}\pi\delta_3\right] \quad \gamma'_1 = \frac{1}{4}\left[\xi_1 - \frac{1}{4}\pi\delta_1\right] \quad \gamma'_2 = \frac{1}{4}\left[-\delta_1 + \frac{1}{4}\pi\xi_1\right] \quad \gamma'_3 = \frac{1}{3}[\xi_2 - \delta_2] \quad \gamma'_4 = -\delta_4 + \xi_4. \tag{13}$$

It should be mentioned that $\xi_i = a_c\hat{\xi}_i,\ \delta_i = a_c\hat{\delta}_i\ i = 1,\ldots,4$, where a_c is the axial depth of cut. Therefore, in next formulation and simulation results, axial depth of cut is included in coefficients $\xi_i,\ \delta_i$. Similarly, the mentioned approach for nonlinear force modeling can be extended to any other machining condition in which cutting force signals are measured experimentally (as it has been discussed for a real case study in [23,43]).

3. Application of the tunable vibration absorber (TVA) for regenerative chatter suppression in machining of plate work-pieces

In this section, the application of a tunable vibration absorber (TVA) for chatter suppression in the milling of plate components is studied. The related formulation is presented in a general configuration, but as the case study considered here, results are investigated for a cantilever plate, as shown in Fig. 3 (which is extensively used in machining processes). There are some practical limitations or requirements that prevent using the fixtures surrounding the plate. First, in many cases of machining, due to the limited operating space of CNC machine, it is not possible to use surrounding fixtures. Second, in the majority of peripheral milling processes, it is exclusively desired to machine the free extremity of the plate. Under these limitations or desired objectives, using industrial fixtures to prevent bending vibrations is impossible. In a previous research [41], TVA was designed for a cantilever plate under the simple harmonic excitation as, $f(t) = F_0\sin\omega t$. In this study, the nonlinear cutting forces in x–y directions, explained by Eq. (12), play as the excitation forces.

During the milling process of plates, for the cases where a cutting tool with relatively short extension part is used, the assumption of SDOF model may not be sufficiently accurate. Although the short cutting tool (with very high natural frequencies) can be considered as a rigid body, plate work-piece is a continuous system and contains infinite number of vibration modes. So, when the control procedure is developed to suppress only the dominating mode, the rest of the structural modes may be excited, resulting in a spill-over problem.

3.1. Vibration specifications of the cantilever plate

Plate structures constitute of an infinite number of degrees of freedom, and the mode summation method is used to model them as the systems consisting of a finite number of more significant degrees of freedom. As shown in Fig. 3(a), a uniform rectangular plate over the domain D defined by $0 < x < L_1$, $0 < y < h$ and $0 < z < L_2$ and clamped in $z = L_2$ is considered (h is the plate thickness). The plate is under the excitation of cutting forces in x–y directions, in correspondence with coordinates shown in Fig. 2. Using the extended Hamilton's principle [44], and assuming the plate deflection $w(x,z,t)$ in x–z plane as $w = W(x,z)\eta(t)$, in which W depends on the spatial coordinates and η is a time-dependent harmonic function of frequency ω, leads to:

$$\nabla^4 W(x,z) - \tilde{\beta}^4 W(x,z) = \eta/D_E \quad \tilde{\beta}^4 = \rho'\omega^2/D_E, \quad x,z \text{ in } D, \tag{14}$$

where ρ' is the mass density, D_E is the plate flexural rigidity defined as $D_E = Eh^3/12(1-\nu^2)$ and E, h, ν are the Young's modulus, plate thickness and Poisson's ratio, respectively. Natural mode shapes of the cantilever plate are found by solving Eq. (14) as:

$$W_{mn}(x,z) = \phi_m(\chi)\,\psi_n(\varsigma), \tag{15}$$

where $\chi = x/L_1$, $\varsigma = z/L_2$. Functions ϕ are found for clamped-free beam function as [45]:

$$\phi_m(\chi) = \mu_m(\cosh\alpha_m\chi - \cos\alpha_m\chi) - \upsilon_m(\sinh\alpha_m\chi - \sin\alpha_m\chi) \quad (m = 1,2,3,\ldots),$$
$$\mu_m = (\cosh\alpha_m + \cos\alpha_m)/(\sinh\alpha_m\sin\alpha_m), \quad \upsilon_m = (\sinh\alpha_m - \sin\alpha_m)/(\sinh\alpha_m\sin\alpha_m), \tag{16}$$

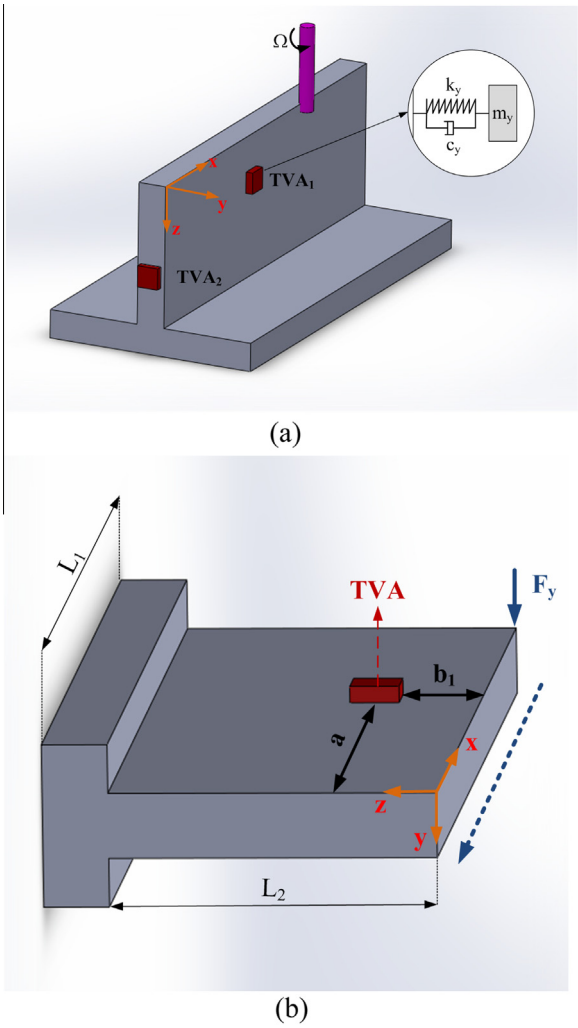

Fig. 3. (a) Schematic of the cantilever plate with attached vibration absorbers in peripheral milling process, (b) application of the TVA for chatter suppression in x–z plane.

where α_m are the roots of characteristic equation, $\cosh\alpha_m\cos\alpha_m=-1$, as $\alpha_1=1.875,\ \alpha_2=4.694,\ \alpha_3=7.854,\ \alpha_4=10.995,\ \alpha_5=14.137,\ldots$. Functions ψ are found for free-free beam function as:

$$\begin{aligned}&\psi_1(\varsigma)=1,\psi_2(\varsigma)=\sqrt{3}(2\varsigma-1),\\&\psi_n(\varsigma)=\bar{\mu}_n(\cosh\beta_n\varsigma+\cos\beta_n\varsigma)-\bar{\upsilon}_n(\sinh\beta_n\varsigma+\sin\beta_n\varsigma)\quad(n=3,4,5,\ldots),\\&\bar{\mu}_n=\frac{\cosh\beta_n-\cos\beta_n}{\sinh\beta_n\sin\beta_n},\quad\bar{\upsilon}_n=\frac{\sinh\beta_n+\sin\beta_n}{\sinh\beta_n\sin\beta_n},\end{aligned}\tag{17}$$

where β_n are the roots of characteristic equation, $\cosh\beta_n\cos\beta_n=1$, as $\beta_3=4.73,\ \beta_4=7.853,\ \beta_5=10.995,\ldots$. In this paper, a square cantilever plate in x–z plane ($L_1/L_2=1$) is used for analysis (similar results can be obtained for other values of L_1/L_2). First five values of the frequency parameter $\omega L_1^2(\rho/D)^{0.5}$ for a cantilever plate are found as 3.49, 8.55, 21.44, 27.46 and 31.17 [45].

3.2. Dynamic model of the plate work-piece with attached vibration absorber

Consider a uniform cantilever plate with a clamped edge in $z=L_2$ as shown in Fig. 3. Transverse deflections of the plate in x–z and y–z planes are expanded as:

$$w(x,z,t)=\sum_{m=1}^{\infty}\sum_{n=1}^{\infty}W_{mn}(x,z)\,\eta_{mn}(t);\quad v(y,z,t)=\sum_{m=1}^{\infty}\sum_{n=1}^{\infty}V_{mn}(y,z)\,\eta'_{mn}(t),\tag{18}$$

where $w(x,z,t)$ and $v(y,z,t)$ are the plate deflections at positions (x,z) and (y,z), respectively. $W_{mn}(x,y)$ and $V_{mn}(y,z)$ are the natural mode shapes of the plate as explained in Section 3.1. $\eta_{mn}(t)$ and $\eta'_{mn}(t)$ are the modal coordinates which satisfy an infinite set of independent modal equations as [44]:

$$\begin{aligned}&\ddot{\eta}_{mn}(t)+\omega_{xz}^2\eta_{mn}(t)=N_{mn}(t);\quad N_{mn}(t)=\int_D W_{mn}(x,z)f(x,z,t)\,dD_{xz},,\\&\ddot{\eta}'_{mn}(t)+\omega_{yz}^2\eta'_{mn}(t)=N'_{mn}(t);\quad N'_{mn}(t)=\int_D V_{mn}(y,z)f'(y,z,t)\,dD_{yz},\quad m,n=1,2,\ldots\end{aligned}\tag{19}$$

As shown in Fig. 3, two vibration absorbers (TVA_1 and TVA_2) consisting of a lumped mass attached to a spring and damper are applied at the positions $(x=a,\ z=b_1)$ and $(y=h/2,\ z=b_2)$, respectively. Cutting forces in y–x directions (F_y and F_x) are exerted at the locations $(0<x=c_1<L_1,\ z=d_1\approx 0)$ and $(0<y=c_2<h,\ z=d_2\approx 0)$, respectively. Mass, spring and damper components of the TVA_1 and TVA_2, in x–z and y–z planes, are denoted by $m_y,\ k_y,\ c_y$ and $m_x,\ k_x,\ c_x$, respectively (they are only shown for TVA_1 in Fig. 3(a)).

The plate deflection at the absorbers locations are denoted by $w(a,b_1,t)$ and $v(h/2,b_2,t)$, respectively. Also, it is denoted by $w(c_1,d_1,t)$ and $v(c_2,d_2,t)$ at the position of y and x cutting forces. In addition, $u(t)$ and $u'(t)$ stands for displacements of the absorbers' mass in x–z and y–z planes, respectively. Referring to Fig. 3 and considering Eq. (19), coupled delay equations for the constrained plate and absorber in the x–z plane are expressed as:

$$\begin{cases}\ddot{\eta}_{mn}(t)+2\zeta_{mn}\omega_{mn}\dot{\eta}_{mn}(t)+\omega_{mn}^2\eta_{mn}(t)=\\ \quad\frac{1}{M}\{F_y(t,\tau)\mathrm{W}_{mn}(c_1,d_1)-c_y[\dot{\mathrm{w}}(a,b_1,t)-\dot{u}(t)]\mathrm{W}_{mn}(a,b_1)-k_y[\mathrm{w}(a,b_1,t)-u(t)]\mathrm{W}_{mn}(a,b_1)\},\\ m_y\ddot{u}(t)+c_y[\dot{u}(t)-\dot{\mathrm{w}}(a,b_1,t)]+k_y[u(t)-\mathrm{w}(a,b_1,t)]=0\end{cases}\tag{20-1}$$

and in y–z plane are expressed as:

$$\begin{cases}\ddot{\eta}'_{mn}(t)+2\zeta'_{mn}\omega'_{mn}\dot{\eta}'_{mn}(t)+\omega'^2_{mn}\eta'_{mn}(t)=\\ \quad\frac{1}{M}\{F_x(t,\tau)\mathrm{V}_{mn}(c_2,d_2)-c_x[\dot{\mathrm{v}}(h/2,b_2,t)-\dot{u}'(t)]\mathrm{V}_{mn}(h/2,b_2)-k_x[\mathrm{v}(h/2,b_2,t)-u'(t)]\mathrm{V}_{mn}(h/2,b_2)\},\\ m_x\ddot{u}'(t)+c_x[\dot{u}'(t)-\dot{\mathrm{v}}(h/2,b_2,t)]+k_x[u'(t)-\mathrm{v}(h/2,b_2,t)]=0,\end{cases}\tag{20-2}$$

where M is the plate mass, $(\zeta_{mn},\ \zeta'_{mn})$ and $(\omega_{mn},\ \omega'_{mn})$ are damping ratio and natural frequencies of the plate in x–z and y–z planes, respectively. Also, in Eq. (20), plate deflections at the absorbers' locations are expanded as:

Table 1
Nominal values for realistic parameters of the system for cutting conditions and milling dynamics [23,24,43].

Cutting conditions	Start and exit immersion angles	Cutter teeth number	Spindle speed	Helix angle	Feed rate per tooth per revolution
	$\phi_{st}=0$ $\phi_{ex}=\pi/2$	$N=4$	$\Omega=625$ rpm	$\beta=30$	$c_f=0.2$ mm/rev-tooth
Cutting force coefficients ($a_c=2.5$ mm)	$\xi_1=6765\ \mathrm{N/mm^3},\ \xi_2=-4910\ \mathrm{N/mm^2},\ \xi_3=2840\ \mathrm{N/mm},\ \xi_4=132$ N $\delta_1=12,740\ \mathrm{N/mm^3},\ \delta_2=-7452\ \mathrm{N/mm^2},\ \delta_3=1674\ \mathrm{N/mm},\ \delta_4=246$ N				

Table 2
Realistic parameters of the cantilever plate.

Plate specification (AL7075)	
Mass per unit area in x–z plane	$\rho_{xz}=56.2\ \mathrm{kg/m^2}$
Mass per unit area in y–z plane	$\rho_{yz}=2810\ \mathrm{kg/m^2}$
Young modulus	$E=71.7\ \mathrm{GN/m^2}$
Poisson's ratio	$\nu=0.33$
Length (x)	$L_1=1$ m
Width (z)	$L_2=1$ m
Thickness (y)	$h=2$ cm

Table 3
First five lower natural frequencies of the cantilever plate (while for the absorber $m_y=2$ kg, $k_y=23$ kN/m).

	Natural frequencies of the plate (rad/s)				
x–z Plane without absorber	107.7	263.9	661.7	847.5	962.1
x–z Plane with absorber	125.7	274.7	667.3	852.3	966.6
y–z Plane without absorber	3860	2.43×10^4	High-order values		

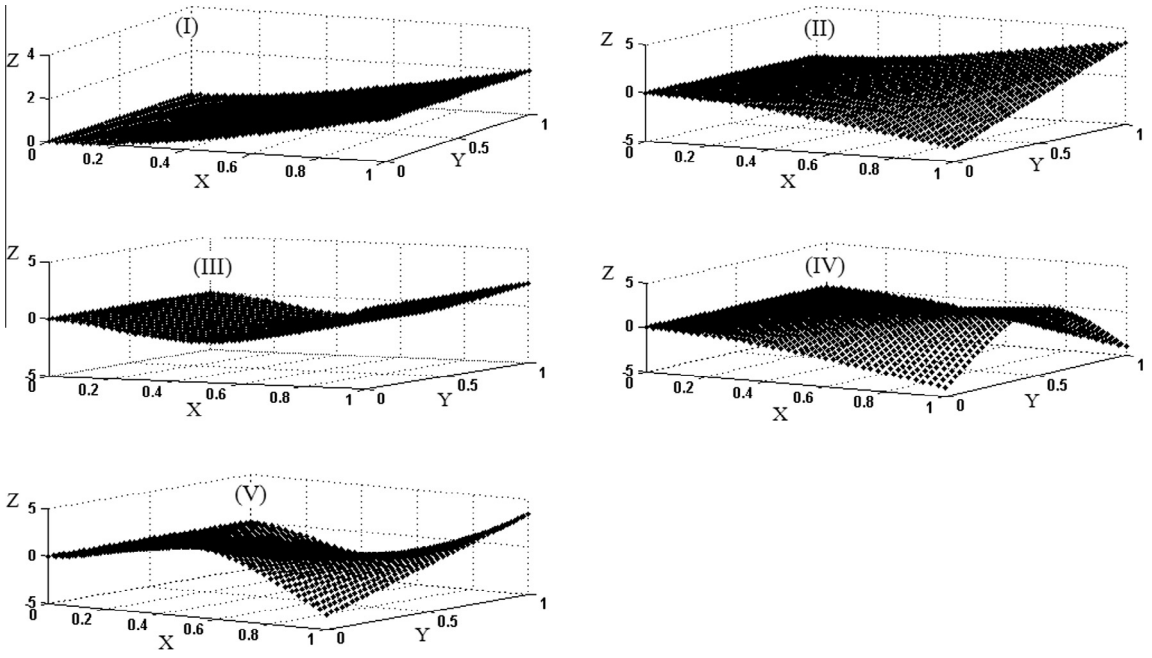

Fig. 4. First five lower mode shapes of the cantilever plate.

$$w(a,b_1,t)=\sum_{r=1}^{\infty}\sum_{s=1}^{\infty}W_{rs}(a,b_1)\,\eta_{rs}(t);\quad v(h/2,b_2,t)=\sum_{r=1}^{\infty}\sum_{s=1}^{\infty}V_{rs}(h/2,b_2)\,\eta'_{rs}(t). \tag{21}$$

Delay terms Δx and Δy for the cutting force $F_y(t)$, given by Eq. (12), are expanded as:

$$\begin{aligned}\Delta x&=\sum_{r=1}^{\infty}\sum_{s=1}^{\infty}\mathrm{V}_{rs}(c_1,0)\,[\eta'_{rs}(t)-\eta'_{rs}(t-\tau)],\\ \Delta y&=\sum_{r=1}^{\infty}\sum_{s=1}^{\infty}\mathrm{W}_{rs}(c_1,0)\,[\eta_{rs}(t)-\eta_{rs}(t-\tau)]\end{aligned} \tag{22}$$

and for the cutting force $F_x(t)$ as,

$$\begin{aligned}\Delta x&=\sum_{r=1}^{\infty}\sum_{s=1}^{\infty}\mathrm{V}_{rs}(h/2,0)\,[\eta'_{rs}(t)-\eta'_{rs}(t-\tau)],\\ \Delta y&=\sum_{r=1}^{\infty}\sum_{s=1}^{\infty}\mathrm{W}_{rs}(h/2,0)\,[\eta_{rs}(t)-\eta_{rs}(t-\tau)].\end{aligned} \tag{23}$$

Under regenerative chatter condition with chatter frequency of ω_c, the modal coordinates $\eta_{ij}(t)$, $\eta'_{ij}(t)$, $ij=mn,\,rs$ and absorbers' displacements $u(t)$, $u'(t)$ can be written in the exponential form as:

$$\eta_{ij}(t)=\bar{\eta}_{ij}e^{J\omega_c t},\quad u(t)=\bar{u}\,e^{J\omega_c t},\quad u'(t)=\bar{u}'\,e^{J\omega_c t},\quad ij=mn,\,rs, \tag{24}$$

where J denotes the imaginary unit. Substituting the above exponential forms in the coupled dynamics of Eq. (20), leads to the system vibration equations as:

$$\begin{cases}\bar{\eta}_{mn}(\omega_{mn}^2-\omega_c^2)+J[2\zeta_{mn}\omega_{mn}\omega_c\bar{\eta}_{mn}+\bar{\Gamma}_y\omega_c\mathrm{W}_{mn}(a,b_1)\sum_{r=1}^{\infty}\sum_{s=1}^{\infty}\mathrm{W}_{rs}(a,b_1)\,\bar{\eta}_{rs}]\\ \qquad+\Gamma_y\mathrm{W}_{mn}(a,b_1)\sum_{r=1}^{\infty}\sum_{s=1}^{\infty}\mathrm{W}_{rs}(a,b_1)\,\bar{\eta}_{rs}-\bar{u}[\Gamma_y\mathrm{W}_{mn}(a,b_1)+J\omega_c\bar{\Gamma}_y\mathrm{W}_{mn}(a,b_1)]=\tilde{F}_y\mathrm{W}_{mn}(c_1,0),\\ \bar{u}\,(\gamma_y+J\omega_c\bar{\gamma}_y-\omega_c^2)-J\omega_c\bar{\gamma}_y\sum_{r=1}^{\infty}\sum_{s=1}^{\infty}\mathrm{W}_{rs}(a,b_1)\,\bar{\eta}_{rs}-\gamma_y\sum_{r=1}^{\infty}\sum_{s=1}^{\infty}\mathrm{W}_{rs}(a,b_1)\,\bar{\eta}_{rs}=0,\end{cases} \tag{25-1}$$

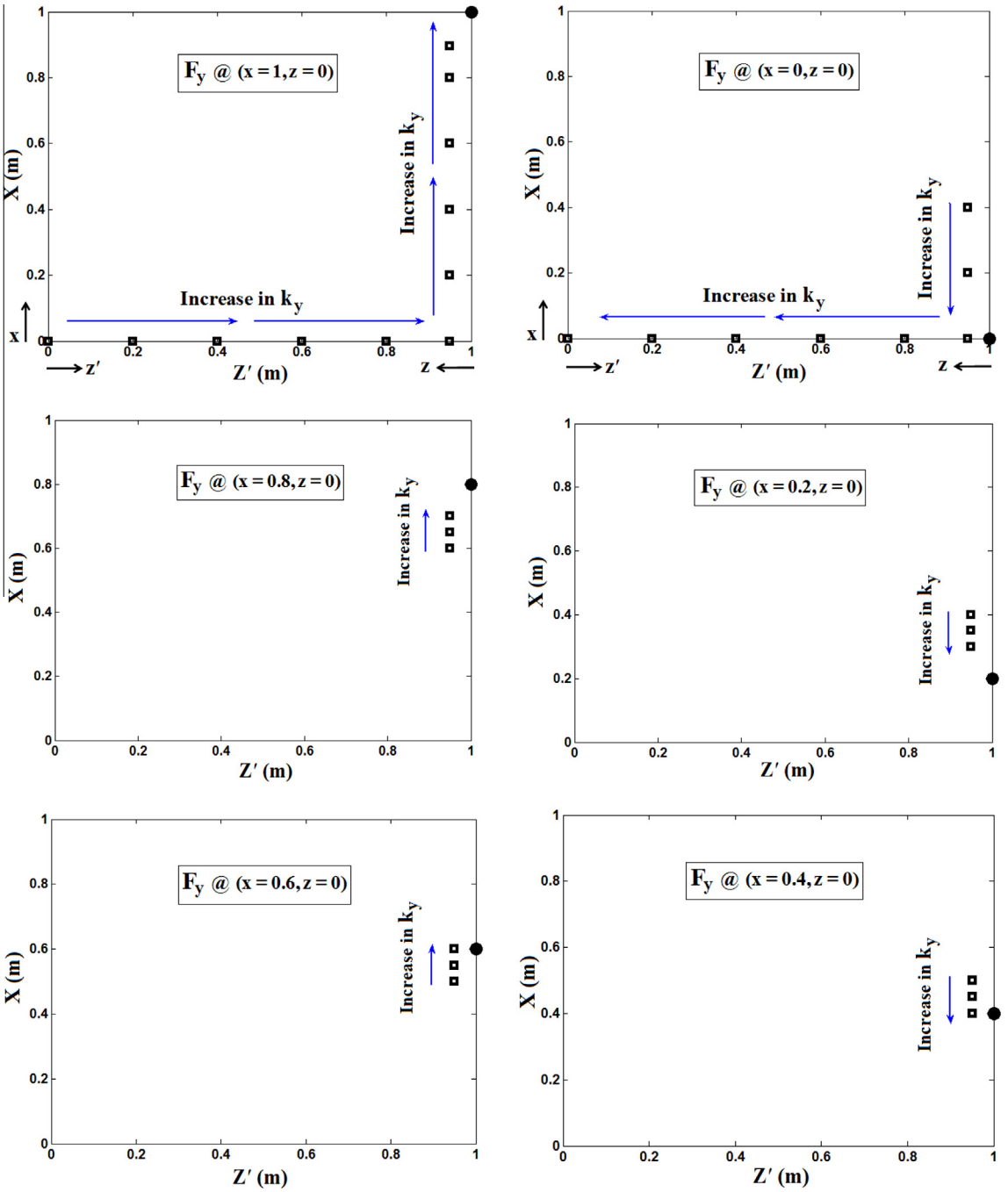

Fig. 5. Best position of the absorber for various values of $1 < k_y < 25$ kN/m (black squares) at different locations of y-direction cutting force (black circle), when $\omega_c = 108$ rad/s $\approx \omega_{n1}$.

$$\begin{cases} \bar{\eta}'_{mn}(\omega'^2_{mn} - \omega_c^2) + J[2\zeta'_{mn}\omega'_{mn}\omega_c\bar{\eta}'_{mn} + \bar{\Gamma}_x\omega_c V_{mn}(h/2,b_2)\sum_{r=1}^{\infty}\sum_{s=1}^{\infty}V_{rs}(h/2,b_2)\bar{\eta}'_{rs}] \\ \quad + \Gamma_x V_{mn}(h/2,b_2)\sum_{r=1}^{\infty}\sum_{s=1}^{\infty}V_{rs}(h/2,b_2)\bar{\eta}'_{rs} - \bar{u}'[\Gamma_x V_{mn}(h/2,b_2) + J\omega_c\bar{\Gamma}_x V_{mn}(h/2,b_2)] = \tilde{F}_x V_{mn}(h/2,0), \\ \bar{u}'(\gamma_x + J\omega_c\bar{\gamma}_x - \omega_c^2) - J\omega_c\bar{\gamma}_x\sum_{r=1}^{\infty}\sum_{s=1}^{\infty}V_{rs}(h/2,b_2)\bar{\eta}'_{rs} - \gamma_x\sum_{r=1}^{\infty}\sum_{s=1}^{\infty}V_{rs}(h/2,b_2)\bar{\eta}'_{rs} = 0, \end{cases} \tag{25-2}$$

where $\Gamma_i = k_i/M,\ \bar{\Gamma}_i = c_i/M,\ \gamma_i = k_i/m_i,\ \bar{\gamma}_i = c_i/m_i$ and $\tilde{F}_i = F_i/M,\ i = x,y$.

It should be noticed that in Eq. (25), cutting forces F_y and F_x are replaced with Eq. (12) in which Δx and Δy are substituted with Eqs. (22) and (23). For the case of absorber with mass and spring elements, equation (25) are reduced by setting $\bar{\Gamma}_i = \bar{\gamma}_i = 0,\ i = x,y$. In addition, for fresh cutting tools with small amount of tool wear, $\xi_4, \delta_4 \approx 0$ and consequently $\gamma_4 = \gamma'_4 \approx 0$ [24]. For the following simulation results, it is assumed that vibration absorbers with mass and spring components and cutting tool with small amount of wear are used.

The coupled dynamics of Eqs. (25-1) and (25-2) are the vibration equations for the combined dynamic system (two equation set for the plate lateral vibrations in x–z and y–z planes and two equations for the vibration absorbers). In the presence of regenerative chatter, this set of equations can be solved numerically via SIMULINK Toolbox of MATLAB. Under regenerative chatter condition, and using Eqs. (22) and (23), Eqs. (25-1) and (25-2) are written in the general matrix form as $[\mathbf{\Lambda}(t,\tau)]\{\mathbf{\Phi}(t,t-\tau)\} = \mathbf{0}$. For $\Re$ number of modes, $[\mathbf{\Lambda}(t,\tau)]$ is a square matrix of order $(4\Re+2)$ which is constituted numerically and

$$
\begin{aligned}
&\{\mathbf{\Phi}(t,t-\tau)\} = \{\bar{\boldsymbol{\eta}}(t) \quad \bar{\boldsymbol{\eta}}'(t) \quad \bar{\boldsymbol{\eta}}(t-\tau) \quad \bar{\boldsymbol{\eta}}'(t-\tau) \quad \bar{u}(t) \quad \bar{u}'(t)\}^T,\\
&\bar{\boldsymbol{\eta}}(t) = [\bar{\eta}_1(t) \ldots \bar{\eta}_{mn=\Re}(t)]_{1\times\Re},\\
&\bar{\boldsymbol{\eta}}(t-\tau) = [\bar{\eta}_1(t-\tau) \ldots \bar{\eta}_{mn=\Re}(t-\tau)]_{1\times\Re},\\
&\bar{\boldsymbol{\eta}}'(t) = [\bar{\eta}'_1(t) \ldots \bar{\eta}'_{mn=\Re}(t)]_{1\times\Re},\\
&\bar{\boldsymbol{\eta}}'(t-\tau) = [\bar{\eta}'_1(t-\tau) \ldots \bar{\eta}'_{mn=\Re}(t-\tau)]_{1\times\Re}.
\end{aligned}
\tag{26}
$$

In the absence of regenerative chatter; the rank of $[\mathbf{\Lambda}(t)]$ is $(2\Re+2)$ because $2\Re$ delay elements including $\bar{\boldsymbol{\eta}}(t-\tau)$ and $\bar{\boldsymbol{\eta}}'(t-\tau)$ are vanished from $[\mathbf{\Lambda}(t,\tau)]$ and $\{\mathbf{\Phi}(t,t-\tau)\}$. Under such conditions without time delay terms, if the determinant of $[\mathbf{\Lambda}(t)]$ is set to zero, $(2\Re+2)$ natural frequencies of the whole system including the plate ($\Re$ natural frequencies in each of x–z and y–z planes) and absorbers are obtained. To achieve the generalized coordinates $\bar{\eta}_{mn}(t)$, $\bar{\eta}'_{mn}(t)$ and the amplitude of the absorbers displacement $\bar{u}$ and $\bar{u}'$, Eqs. (25-1) and (25-2) which includes $(2\Re+2)$ coupled equations must be solved simultaneously.

Finally, it should be noticed that the necessity of nonlinear cutting force modeling is due to the nature of machining processes. In this paper, a nonlinear cutting force model is used because nonlinear modeling of cutting forces in terms of chip thickness is more accurate than the linear one (more details are presented in [23,43]). Therefore, advanced nonlinear model just provides a more accurate model of the process. It does not necessarily lead to the better design of absorber. Moreover, the absorber is designed for the nonlinear model of cutting forces (Eq. (7)). However, if under some specific machining conditions, cutting forces demonstrate a linear behavior (i.e., $\xi_i, \delta_i,\ i = 1,2$ approach zero values), then all presented formulation and design are valid in a more straightforward manner (it is sufficient to fix the mentioned coefficients at zero values).

4. Simulation of the problem, results and discussion

4.1. Practical remarks on simulation of the problem

In this section and as the case study, half immersion up-milling with $\phi_{st} = 0$ and $\phi_{ex} = \pi/2$, four teeth $N = 4$, spindle speed $\Omega = 625$ rpm, helix angle $\beta = 30$, axial depth of cut $a_c = 2.5$ mm and feed rate $c_f = 0.2$ mm/rev-tooth are considered for machining conditions. Moreover, coefficients in nonlinear model of cutting forces, $\xi_i, \delta_i\ i = 1,\ldots,4$, are given in Table 1 [23,24,43]. For simulation of the problem, realistic parameters of the plate work-piece (of AL7075 alloy material), are given in Table 2. In addition, five number of modes $\Re = 5$ is considered for the analysis. This value is selected such that the run times for next algorithms based on mode summation and semi-discretization approaches, become reasonable.

Table 4
Design for the best position of absorber $(a,\ b_1)$ for various locations of the cutting force in y-direction $(0 < c_1 < L_1 = 1\text{ m},\ d_1 \approx 0)$, under regenerative chatter with resonance conditions (for the absorber: $m_y = 2$ kg, $k_y = 23$ kN/m).

Resonance conditions (rad/s)	Location of cutting force in y-direction (m)	Best position of the absorber (m)	
	(c_1 : variable, $d_1 = 0$)	$x = a$	$z = b_1$
$\omega_c \approx \omega_{n1}$	$0.5 \leqslant c_1 \leqslant 1$	0.6	0.05
$\omega_c \approx \omega_{n2}$	$0 \leqslant c_1 < 0.5$	0.4	0.05
$\omega_c \approx \omega_{n3}$	$0.75 \leqslant c_1 \leqslant 1$	0	0.05
	$0.5 \leqslant c_1 < 0.75$	1	0.05
	$0.25 \leqslant c_1 < 0.5$	0	0.05
	$0 \leqslant c_1 < 0.25$	1	0.05
$\omega_c \approx \omega_{n4}$	$0.5 \leqslant c_1 \leqslant 1$	1	0.05
	$0 \leqslant c_1 < 0.5$	0	0.05
$\omega_c \approx \omega_{n5}$	$0.5 \leqslant c_1 \leqslant 1$	0	0.05
	$0 \leqslant c_1 < 0.5$	1	0.05

In previous researches [23,43], the small value of axial depth of cut ($a_c = 2.5$ mm) was used in cutting experiments to evaluate the coefficients of cutting forces (i.e., for extraction of ξ_i, δ_i, $i = 1,\ldots,4$ in Table 1). This parameter extraction can be accomplished at other larger values of depth of cut (while the stability is still guaranteed). However, the same coefficients will be extracted [2,3,42]. Therefore, $a_c = 2.5$ mm is the nominal value used in simulations.

In practice, periodic cutting loads cause cyclic mechanical and thermal stresses on the tool, which diminishes the tool life. To dampen the sharp variations in the oscillatory components of the milling forces, helical end mills are preferred [42]. However, presented formulation is independent of the helix angle (β). This angle value only affects the cutting force coefficients

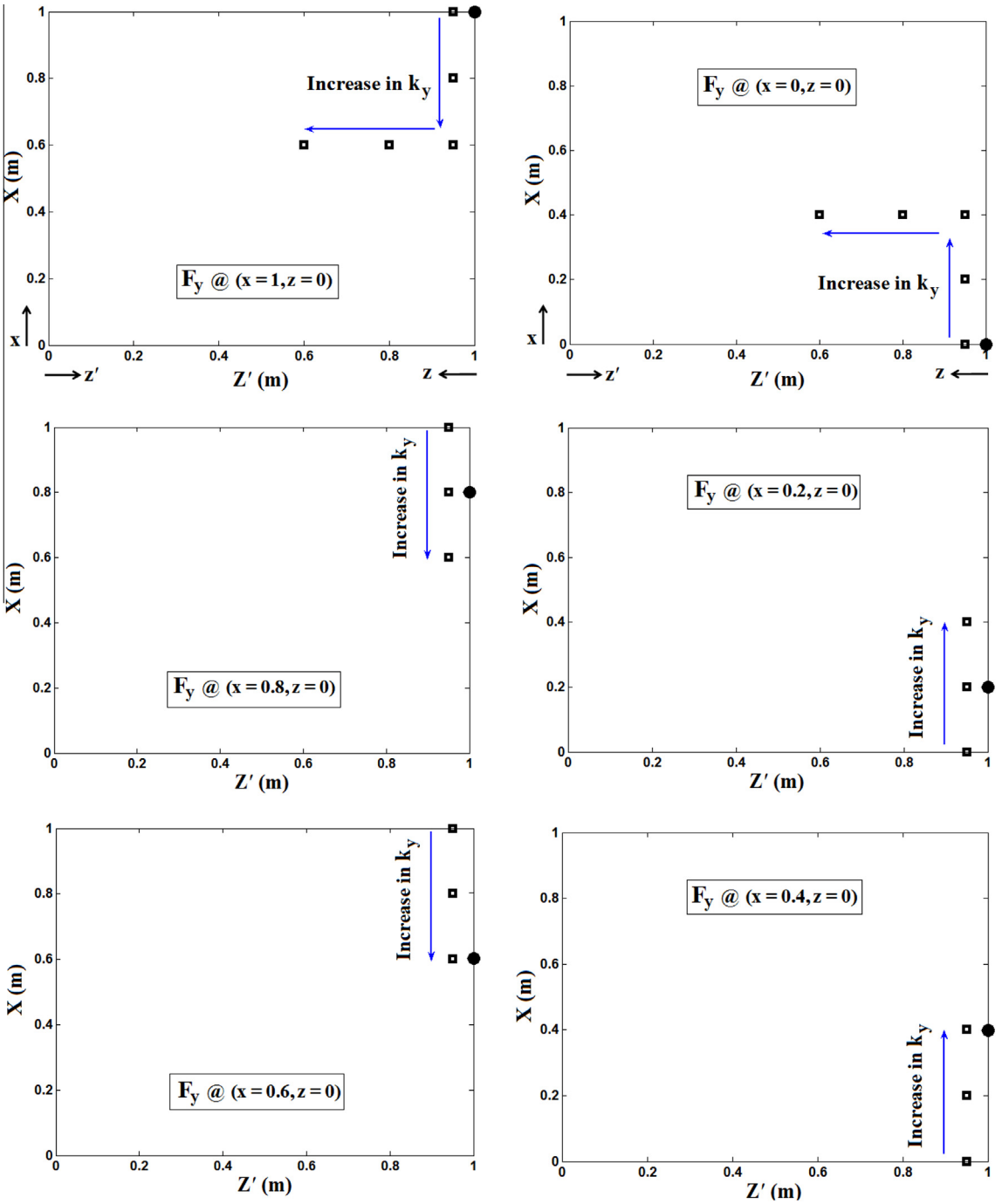

Fig. 6. Best position of the absorber for various values of $1 < k_y < 25$ kN/m (black squares) at different locations of y-direction cutting force (black circle), when $\omega_c = 264$ rad/s $\approx \omega_{n2}$.

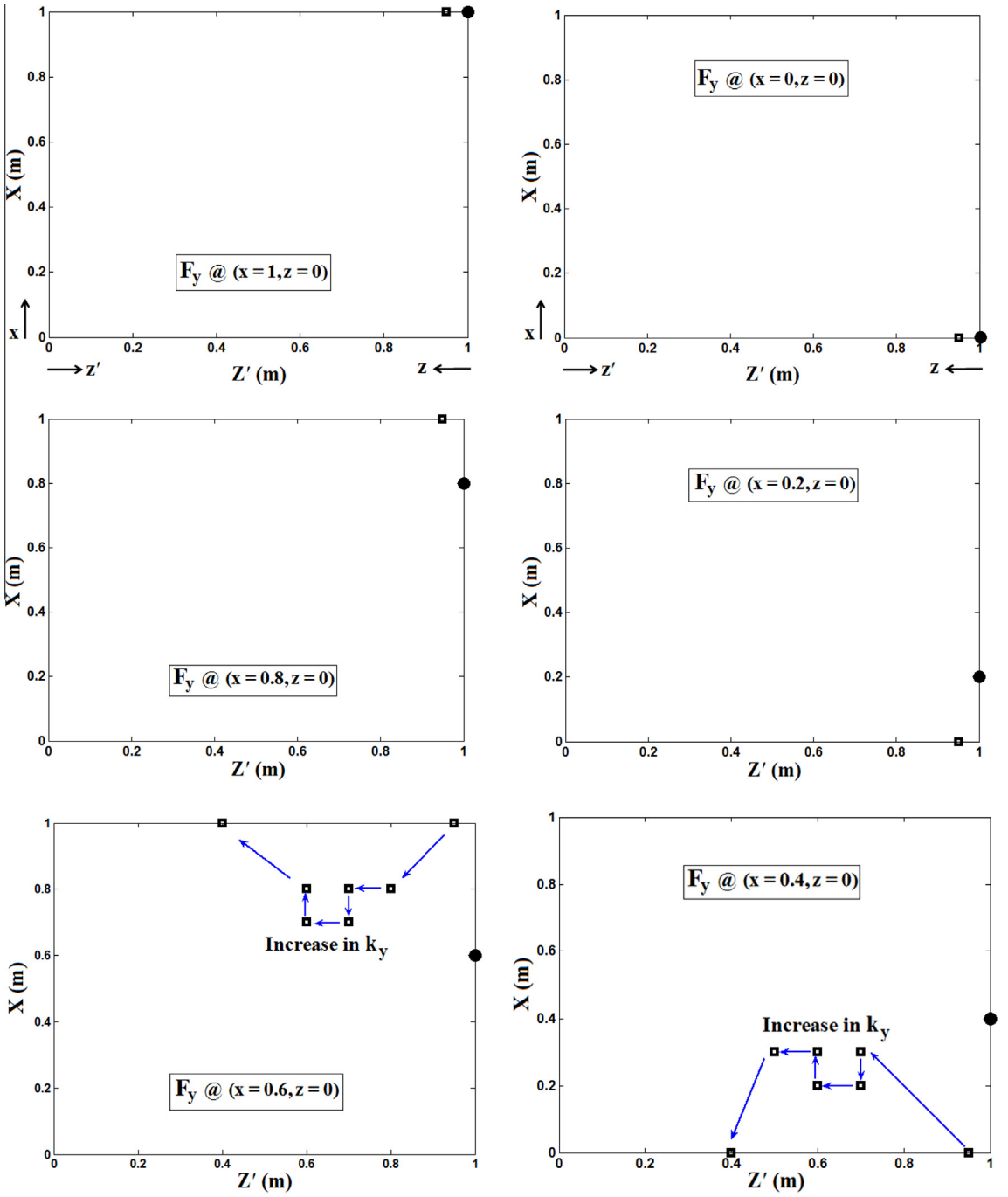

Fig. 7. Best position of the absorber for various values of $1 < k_y < 25$ kN/m (black squares) at different locations of y-direction cutting force (black circle), when $\omega_c = 848$ rad/s $\approx \omega_{n4}$.

ξ_i, δ_i, $i = 1, \ldots, 4$, given in Table 1. Therefore, the procedure of absorber design is also valid for the cutting tools with straight teeth ($\beta = 0$).

As it is presented in Table 3, and expected physically, natural frequencies of the y–z plane are much higher than those of x–z plane (the first natural frequency of y–z plane, $\omega_1' = 3860$, is about four times of the fifth natural frequency of x–z plane, $\omega_5 = 962$ rad/s). It indicates that for machining conditions where the x–z plane is under resonance conditions, y–z plane experience the non-resonance status. Therefore, next simulation results are presented for tunable vibration absorber design (TVA_1) for chatter suppression in the main flexible plane, i.e., x–z plane. It should be mentioned that for machining of

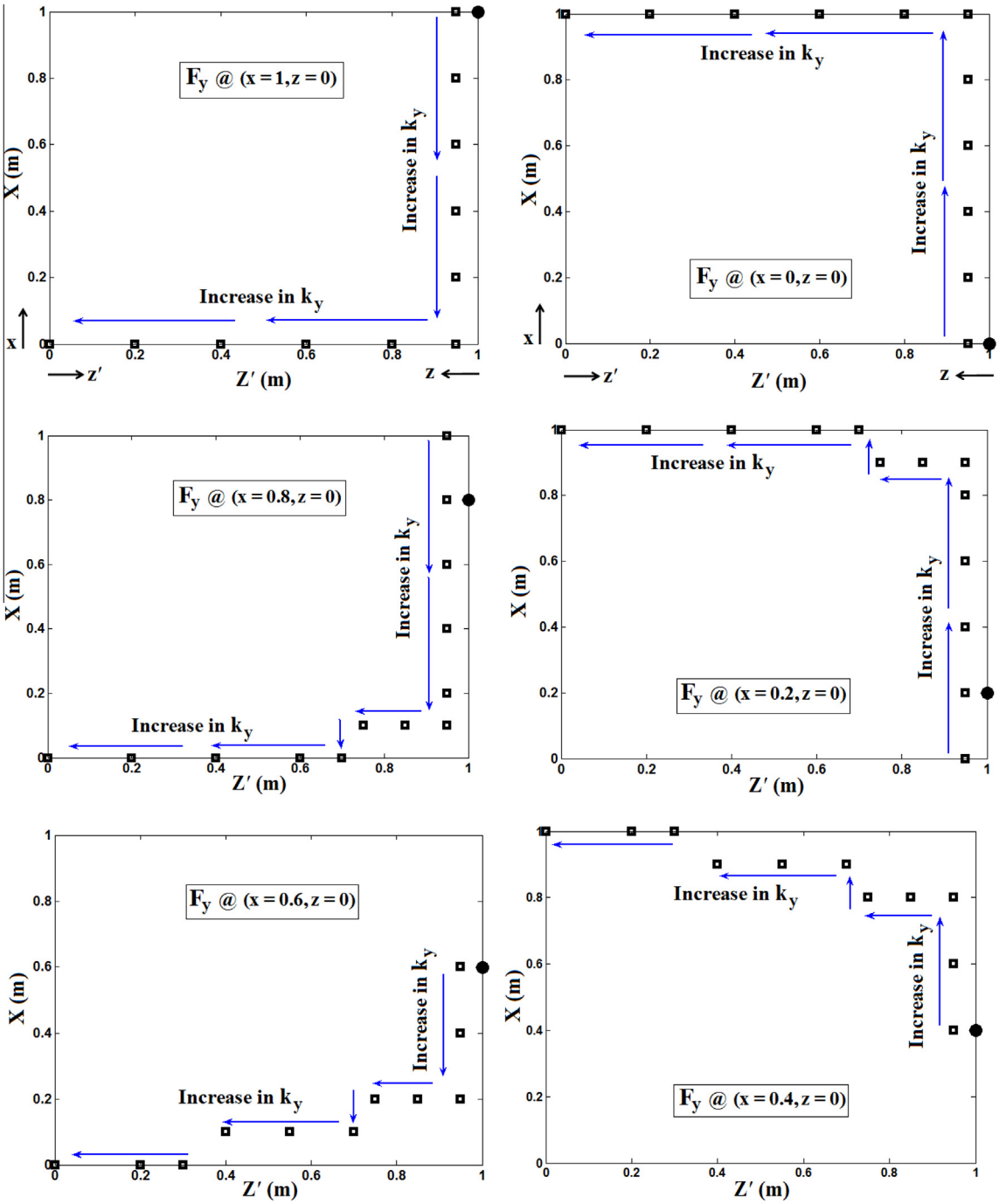

Fig. 8. Best position of the absorber for various values of $1 < k_y < 25$ kN/m (black squares) at different locations of y-direction cutting force (black circle), when $\omega_c \ll \omega_{n1}$ (e.g., $\omega_c = 70$ rad/s).

cantilever plates, where natural frequencies of x–z and y–z planes are of the same order, design of both TVA_1 and TVA_2 must be accomplished according to the complete formulation presented in Section 3.2.

Under resonance conditions, tooth passing frequency (4Ω) approaches the values of natural frequencies in x–z plane. Therefore, according to the values presented in Table 3, resonance occurs in the range of $1000 < 4\Omega < 10,000$ rpm. Consequently, for very high speed machining conditions, more number of modes ($\Re > 5$) must be considered for analysis. First five mode shapes of the cantilever plate in x–z plane are shown in Fig. 4.

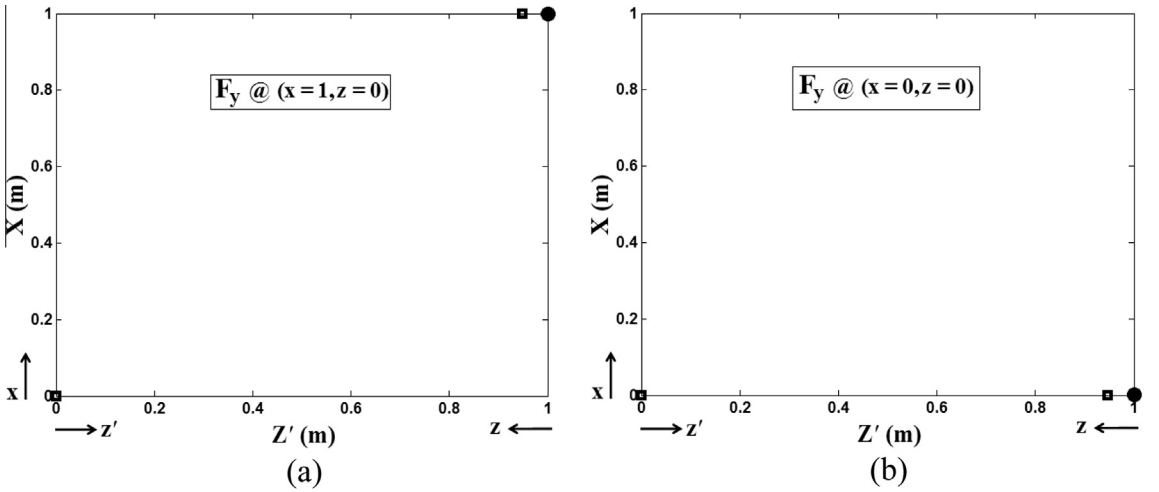

Fig. 9. Best position of the absorber for various values of $1 < k_y < 25$ kN/m (black squares) while cutting force in y-direction is exerted at (a) $x = 1,\ z = 0$ and (b) $x = 0,\ z = 0$ (black circle), when $\omega_{n1} \ll \omega_c \ll \omega_{n2}$ e.g., ($\omega_c = 180$ rad/s). Similar results to the case (a) is obtained when F_y is exerted at ($x = 0.8,\ z = 0$) or ($x = 0.6,\ z = 0$) and similar results to the case (b) is obtained when F_y is exerted at ($x = 0.2,\ z = 0$) or ($x = 0.4,\ z = 0$).

Table 5
Design for the best position of absorber ($a,\ b_1$) for various locations of the cutting force in y-direction ($0 < c_1 < L_1 = 1$ m, $d_1 \approx 0$), under regenerative chatter with non-resonance conditions (for the absorber: $m_y = 2$ kg, $k_y = 12.6$ kN/m).

Resonance conditions (rad/s)	Location of cutting force in y-direction (m)	Best position of the absorber (m)	
	(c_1 : variable, $d_1 = 0$)	$x = a$	$z = b_1$
$\omega_c \ll \omega_{n1}$	$0 \leqslant c_1 \leqslant 1$	0.5	0.05
$\omega_{n1} \ll \omega_c \ll \omega_{n2}$	$0.5 \leqslant c_1 \leqslant 1$	1	0.05
$\omega_{n3} \ll \omega_c \ll \omega_{n4}$	$0 \leqslant c_1 < 0.5$	0	0.05
$\omega_c \gg \omega_{n5}$			
$\omega_{n2} \ll \omega_c \ll \omega_{n3}$	$0.5 \leqslant c_1 \leqslant 1$	0	0.05
$\omega_{n4} \ll \omega_c \ll \omega_{n5}$	$0 \leqslant c_1 < 0.5$	1	0.05

Finally, the following simulation results can be extended and presented for any other machining condition; in which dynamic parameters of the system are identified.

4.2. Structure of the algorithm to optimize the absorber's specification

In this section, an optimal algorithm is developed based on trial and error search on the space of dynamic parameters. In this algorithm, optimum values of the absorber position and its spring stiffness (as control parameters) are found such that plate deflection is minimized under various machining conditions. The value of absorbers' mass is kept constant.

For this purpose, the plate is diffracted into a finite number of square elements (e.g., 20×20 elements) in x and z directions. Then, the absorber is moved along the plate by being placed at the nodes of successive elements. As the absorber is fixed in a node, the midpoint deflection of all plate elements is computed. This procedure is repeated for other next nodes as the absorber is fixed there (20×21 nodes). Finally, among all the values for the absorber position, its best position is the one that the corresponding computed midpoint deflections of elements minimize the following index:

$$\Upsilon = \sum_{n=1}^{20\times 20} \tilde{w}_n^2, \tag{27}$$

where $\tilde{w}_n$ is the midpoint deflection of the nth-element after using the absorber. It should be mentioned that the proposed search for the best values of the absorbers' position can be done for the best values of the springs' stiffness (while other parameters are kept constant). Moreover, this procedure can be performed with an optimum search on both values of springs' stiffness and absorbers' position, simultaneously.

4.3. Optimum design of the absorber under regenerative chatter with resonance & non-resonance conditions

In this section, best position of the absorber and its spring stiffness are found such that plate deflection is minimized. Results are presented and compared for two cases, regenerative chatter under resonance and non-resonance conditions.

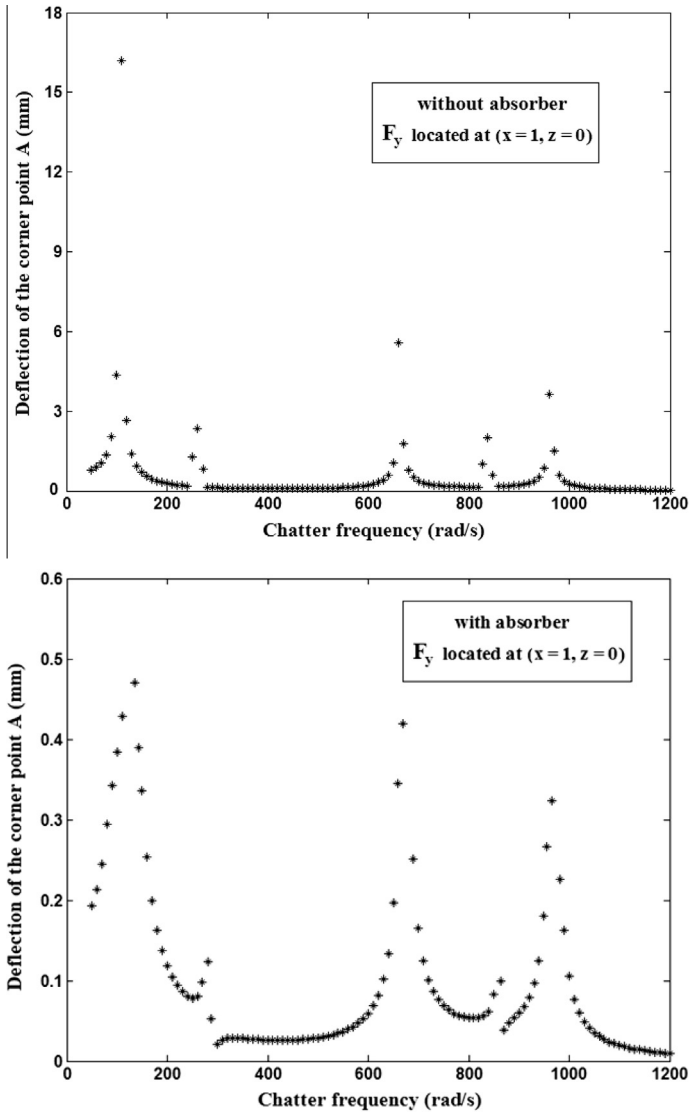

Fig. 10. Frequency response of the free-corner point A ($x = 1,\ z = 0$) under the regenerative chatter condition while cutting force is also exerted at ($x = 1,\ z = 0$) (a) without absorber and (b) with absorber.

Under resonance conditions, chatter frequency (ω_c) approaches one of the natural frequencies of x–z plane, presented in Table 3. In the next simulation results, it is assumed that chatter frequency has been determined by one of the experimental chatter detection approaches, e.g., [46–48], or with the procedure explained in Appendix A. Absorber mass is assumed to be fixed at $m_y = 2$ kg. Also, it is assumed that the external surface of the work-piece is coated with a thin magnetic layer (while the absorbers are also magnetic for attachment to the work-piece).

To find the optimum values of absorbers' specifications, spring stiffness value is changed in the region $1 < k_y < 25$ kN/m (e.g., with $\Delta k_y = 250$ N/m). According to Fig. 3(b), the cutting force in y-direction (F_y) moves along the line ($0 < x = c_1 < 1$ m & $z = d_1 \approx 0$) while the allowable position of TVA_1 is $0 < a < 1$ m and $0 < b_1 < 0.95$ m (0.05 m away from the cutting section). In the following results and for the simplicity, the coordinate z' is defined from the cantilever end of plate, such that $z + z' = L_2 = 1$ m.

Fig. 5 shows the best values of absorber position for various values of spring stiffness while $\omega_c = 108$ rad/s $\approx \omega_{n1}$. Results are presented for different locations of cutting force F_y along the path of movement ($c_1 = \{1,\ 0.8,\ 0.6,\ 0.4,\ 0.2,\ 0\},\ d_1 = 0$). It should be noticed that in this figure and following similar plots, each determined point of absorber location (black squares) is corresponding to several values of spring stiffness. It means that for several values of the k_y, the algorithm predicts a same position for the absorber (such that the Υ-index for plate deflection is minimized). The arrows are used to show the direction of increase in spring stiffness (from $k_y = 1$ to $k_y = 25$ kN/m).

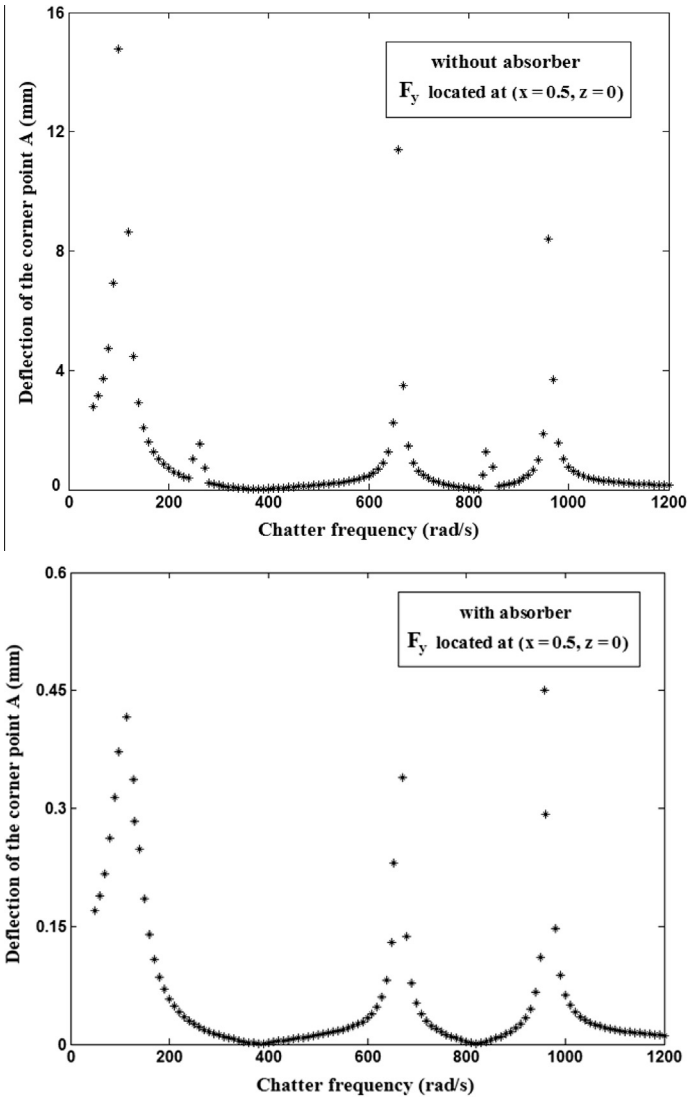

Fig. 11. Frequency response of the free-corner point A $(x = 1,\ z = 0)$ under the regenerative chatter condition while cutting force is exerted at $(x = 0.5,\ z = 0)$ (a) without absorber and (b) with absorber.

As Fig. 5 shows, for different locations of the cutting force, various positions of the absorber are predicted at various values of the spring stiffness. To make the design more convenient, the intersection of predicted results for various plots of Fig. 5, is considered as the optimum design. Therefore, according to Fig. 5 (left column), when the cutting force moves along the path of $(0.5 \leqslant c_1 \leqslant 1,\ d_1 \approx 0)$, the absorber with determined $k_y = 23$ kN/m must be located at $(a = 0.6,\ b_1 = 0.05$ m). For the cutting force path $(0 \leqslant c_1 < 0.5,\ d_1 \approx 0)$, i.e., right column of Fig. 5, the absorber must be located at $(a = 0.4,\ b_1 = 0.05$ m). For this switch control law in position, practically two magnetic absorbers with the specifications of $m_y = 2$ kg, $k_y = 23$ kN/m, can be provided in the proposed positions. Then, depending on the position of cutting force, one of them can be activated to suppress regenerative chatter. The above optimum specifications of the absorber location (for $\omega_c \approx \omega_{n1}$) is given in Table 4.

Best values of the absorber position for various values of spring stiffness, while $\omega_c = 264$ rad/s $\approx \omega_{n2}$ and $\omega_c = 848$ rad/s $\approx \omega_{n4}$, are shown in Figs. 6 and 7, respectively. For the sake of brevity, similar results for the resonance cases $\omega_c \approx \omega_{n3}$ and $\omega_c \approx \omega_{n5}$, are not shown. It should be noticed that under some machining conditions, e.g., first plot of Fig. 7, only one optimum location for the absorber position may be predicted (for all values of k_y). With a similar analysis as that done for the case of $\omega_c \approx \omega_{n1}$ in Fig. 5, optimum specifications of the absorber location for other resonance conditions under regenerative chatter $(\omega_c \approx \omega_{ni},\ i = 2, \ldots, 5)$ are found and presented in Table 4.

Figs. 8 and 9 show the best values of absorber position for various values of spring stiffness, under non-resonance conditions of $\omega_c \ll \omega_{n1}$ e.g., $(\omega_c = 70$ rad/s) and $\omega_{n1} \ll \omega_c \ll \omega_{n2}$ e.g., $(\omega_c = 180$ rad/s), respectively. It should be mentioned that similar results are obtained for other values of ω_c while $\omega_c \ll \omega_{n1}$ or $\omega_{n1} \ll \omega_c \ll \omega_{n2}$, which are not shown.

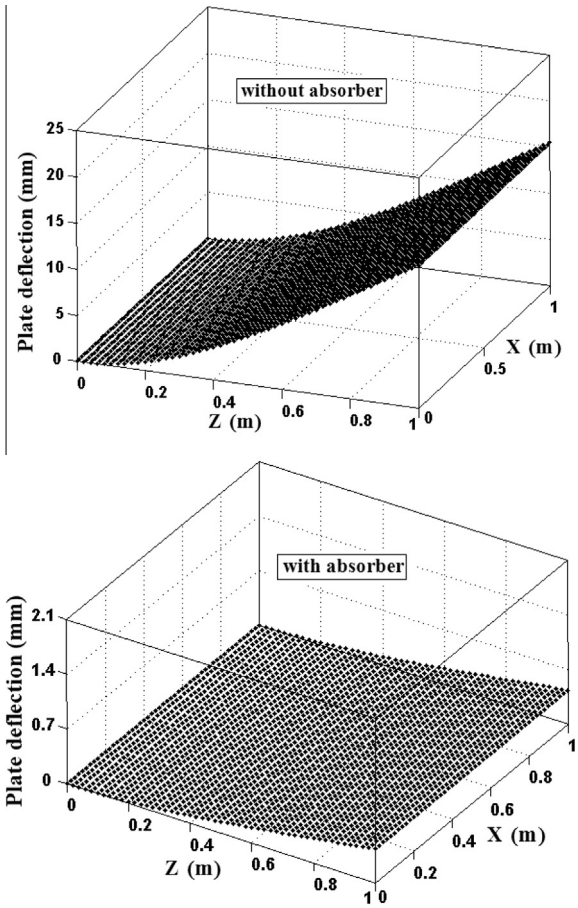

Fig. 12. Plate deflection under the regenerative chatter with resonance condition of $\omega_c = 108$ rad/s $\approx \omega_{n1}$, while the cutting force in y-direction is exerted at $(c_1 = 0.5,\ d_1 = 0)$ (a) without absorber and (b) with absorber.

As it is shown in Fig. 8, under this non-resonance condition, the predicted optimum position of absorber is more sensitive to the values of k_y (i.e., more optimum locations are predicted in comparison with some other cases, e.g., Figs. 6 or 9). Similar results are not presented for other non-resonance conditions, $\omega_{ni} \ll \omega_c \ll \omega_{nj},\ i = 2,3,4;\ j = 3,4,5$ and $\omega_c \gg \omega_{n5}$. Under regenerative chatter with non-resonance conditions, optimum specifications of the absorber location are presented in Table 5 (while the absorber stiffness is determined as $k_y = 12.6$ kN/m). Design presented in Table 5 is performed with a similar procedure as discussed for the resonance case of $\omega_c \approx \omega_{n1}$, in Fig. 5.

It should be noticed that in this research, the work-piece plate is clamped at one edge all over the whole machining process. Moreover, during the machining, the cutting tool moves along a fixed path, i.e., top free edge of the work-piece (Fig. 3). Under such machining conditions, only the geometrical parameter (L_2) is variable. Consequently, natural frequencies of the plate are changed. But, the developed algorithm predicts the same optimized values of absorber location (generally, with similar behavior observed in Figs. 5–9). For the sake of brevity, similar simulation results are not presented (when L_2 is decreased). However, it should be noticed that if the cutting tool path becomes variable in each passes of cut, presented design may be failed along some specific paths. Under such condition, development of the online control strategies (active controls) is mandatory.

4.4. Chatter suppression via optimum vibration absorber

In the previous section, optimum values of the absorber parameters were found as $m_y = 2$ kg, $k_y = 23$ kN/m and $m_y = 2$ kg, $k_y = 12.6$ kN/m for resonance and non-resonance cases, respectively. Also best position of the absorber, for a wide range of chatter frequencies, is presented in Tables 4 and 5. Frequency response of an arbitrary point, e.g., point A located at the free-corner of plate $(x = 1,\ z = 0)$, is shown in Figs. 10 and 11 (with/without the absorber). In these figures, the cutting force (F_y) is exerted at the corner $(x = 1,\ z = 0)$ and midpoint $(x = 0.5,\ z = 0)$ of plate's free edge, respectively. Similarly, other frequency responses can be obtained for various points of the plate, while the cutting force is moving along the path $(0 < x = c_1 < 1$ m & $z = d_1 \approx 0)$, which are not shown. As it is shown in Figs. 10 and 11, optimum absorber acts efficiently in chatter reduction, especially around the natural frequencies of the plate (resonance conditions). For instance,

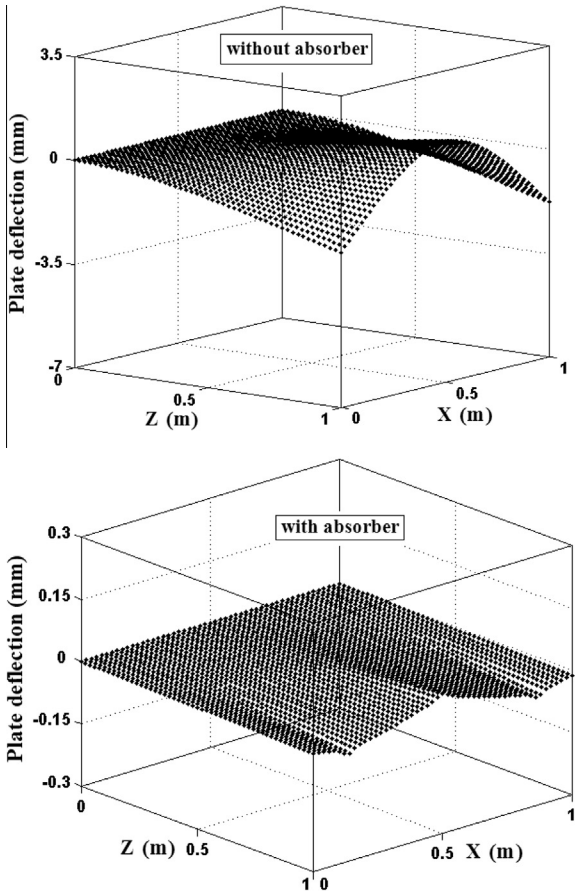

Fig. 13. Plate deflection under the regenerative chatter with resonance condition of $\omega_c = 848$ rad/s $\approx \omega_{n4}$, while the cutting force in y-direction is exerted at $(c_1 = 0.5,\ d_1 = 0)$ (a) without absorber and (b) with absorber.

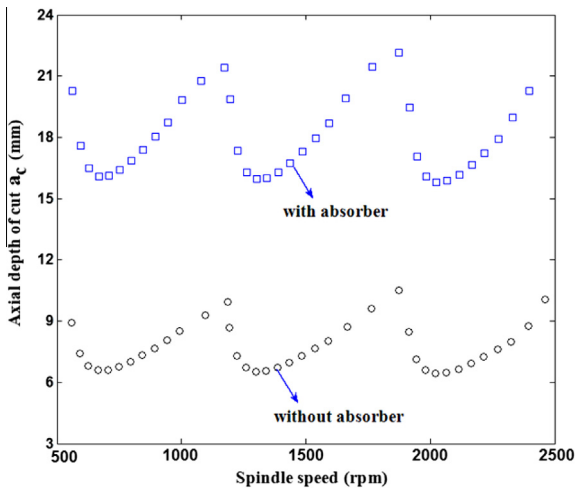

Fig. 14. Stability lobes diagram of the process without (black circles) and with (blue squares) vibration absorber. (For interpretation of the references to color in this figure legend, the reader is referred to the web version of this article.).

comparing the plots of Fig. 10 reveals that TVA reduces the vibration amplitudes about $TR_1 = 34$, $TR_2 = 19$, $TR_3 = 14$, $TR_4 = 20$ and $TR_5 = 12$ times around resonance conditions $\omega_c \approx \omega_{ni},\ i = 1, \ldots, 5$.

Figs. 12 and 13 show the effect of optimum absorber in chatter suppression of the plate around the first and fourth natural frequencies (not shown for other resonance/non-resonance cases). In these figures, the cutting force (F_y) is exerted at the midpoint ($x = 0.5,\ z = 0$) of plate's free edge. As it is shown, designed absorber acts effectively in chatter suppression of the plate work-piece (this desired objective was defined by Eq. (27)).

4.5. Improvement in stability lobes diagram after implementation of the TVA

Stability of any machine-tool system can be shown in the diagrams in which the effects of axial depth cut, cutting velocity and other machining parameters on stability are analyzed. In stability lobes diagram, the margins between stable and unstable conditions are shown with several lobes for various conditions of axial depth of cut and spindle speed.

In this section, to investigate the milling stability, semi-discretization method (SDM) is used. Due to the similarity in general formulation of SDM to the one presented in [12], it is not developed in this paper. In the research [12], SDM was applied on the nonlinear model of cutting forces in the milling process, where the extension part of cutting tool was modeled as an Euler–Bernoulli beam. In analogous with that formulation, SDM can be applied here for the stability analysis in machining of plate work-piece (as a continuous system).

SDM technique is often used in computational fluid mechanics for solving partial differential equations (PDEs). In this approach, the PDE is discretized along the spatial coordinates while the time coordinate are kept unchanged. Similarly, this method was applied for the analysis of delay differential equations (DDEs); where delayed terms are approximated by piecewise constant functions while the current time terms are kept unchanged [7,8]. Therefore, DDE is approximated by a series of ordinary differential equations (ODEs).

Following SDM, stability lobes diagrams of the process with/without absorber are shown in Fig. 14. As it is observed, optimum TVA improves the stability limits with a considerable increase in the critical value of depth of cut. Therefore, after implementation of TVA, larger values of axial depth of cut and consequently higher material removal rate (MRR) can be achieved, without moving to the unstable conditions.

Finally, it should be mentioned that in this research, the absorber just recognizes the occurrence of unstable large vibration amplitudes. Here, this instability is caused by regenerative chatter in machining process. It may be arisen by other sources of instability in other applications such as the existence of random excitation (e.g., the plates under wind excitation or floating platforms under ocean/sea wave excitation). Therefore, the presented absorber design for plate work-pieces can be extended to other industrial applications; while the type of excitation and sources of instability are varied among them. Moreover, it should be noticed that under broadband random excitations, the frequency contain of the excitation may be changed. Consequently, more number of modes must be considered in the design procedure. However, after recognition of dominant modes, it is possible to follow the absorber design for the less number of dominant modes.

5. Conclusions

In this paper, an extended model of the milling process with nonlinear regenerative chatter effect in cutting forces is considered. A tunable vibration absorber (TVA), as a semi-active control approach, is designed for chatter suppression in the milling of plate work-pieces. Unlike the previous researches of this area, in which the cutting tool and work-piece were modeled as flexible and rigid body parts, the short cutting tool is assumed to be rigid while the plate work-piece is the flexible component. Plate work-piece vibration, caused by nonlinear cutting forces with regenerative chatter effect, is suppressed after implementation of the TVA.

In the presence of nonlinear regenerative chatter with associated time delay terms, the extensive formulation of the process including the plate and attached absorber is presented. Optimum values of the absorber position and its spring stiffness are found such that the plate vibration is minimized (while the absorber mass is kept constant). For this purpose, an optimal algorithm based on mode summation technique and auxiliary algorithms via SIMULINK Toolbox of Matlab, are developed. Simulation results are presented and compared for two cases: regenerative chatter under resonance and non-resonance conditions. It is observed that for both machining conditions and in a wide range of chatter frequencies, TVA guarantees chatter suppression effectively. For this evaluation, results are investigated through frequency response functions and plate deflections (with/without absorber).

Using semi-discretization method (SDM), stability lobes diagrams of the process with/without absorber are constructed. It is shown that using TVA also improves stability limits of the process. Therefore, larger values of depth of cut and consequently more material removal rate can be obtained after implementation of the TVA (while the process stability is guaranteed simultaneously). In comparison with other control approaches, proposed TVA design includes some great advantages such as simple design, intuitive clarity, reduction in hardware and development cost.

Acknowledgment

The authors acknowledge the 'National Elite Foundation' of Iran for supporting this research

Appendix A

In this paper, it is assumed that chatter frequency has been detected by one of the experimental chatter detection approaches, e.g., [46–48]. In these methods, chatter frequency is usually determined by analysis of measured signals such as: audio, spindle drive current, tool tip acceleration and cutting forces. This signal analysis is accomplished in time or frequency domains or a combination of them. However, in the simulation results of this paper, chatter frequency is determined from time analysis of the plate displacements. For this purpose, a trial and error based algorithm is developed via SIMULINK Toolbox of MATLAB. For various spindle speeds and consequently chatter frequencies, dynamics of the system with/without absorber, given by Eq. (20), is simulated. Axial depth of cut is increased gradually until reaching unstable conditions. The corresponding unstable time response of the plate deflection (in an arbitrary point) is analyzed. Accordingly, chatter frequency is determined at the considered spindle speed.

For instance, Fig. A.1 shows the unstable time response of free-corner point (point B) of the plate located at ($x = 0,\ z = 0$), while $\Omega = 625$ rpm and critical axial depth of cut is $a_c = 6.8$ mm. According to the simulated signal, chatter frequency is determined as $\omega_c = 258$ rad/s. Similarly, for other values of the spindle speed, the same analysis can be done to find the chatter frequency. Fig. A.2 shows the time response of the same point B ($x = 0,\ z = 0$), after implementation of the designed optimum absorber (while $\Omega = 625$ rpm). As it is observed, using TVA leads to the stable machining conditions.

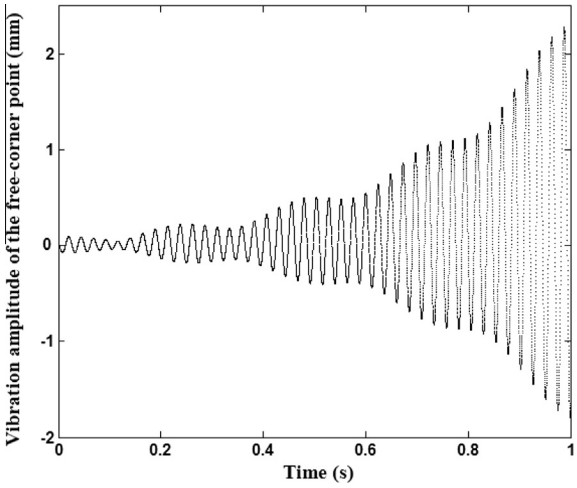

Fig. A.1. Vibration amplitudes of the free-corner point of the plate located at ($x = 0,\ z = 0$) with the spindle speed of $\Omega = 625$ rpm and critical axial depth of cut $a_c = 6.8$ mm.

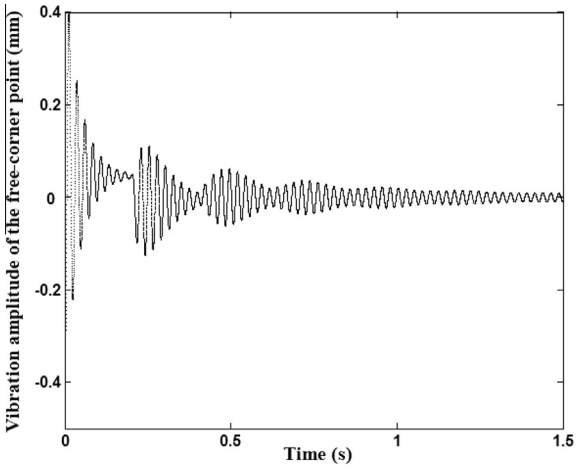

Fig. A.2. Vibration amplitudes of the free-corner point of the plate located at ($x = 0,\ z = 0$) after implementation of the absorber, with the spindle speed of $\Omega = 625$ rpm and axial depth of cut $a_c = 6.8$ mm.

References

[1] H.E. Merrit, Theory of self excited machine-tool chatter: contribution to machine-tool chatter research, Trans. ASME J. Eng. Ind. B87 (4) (1965) 447–454.
[2] F. Koenigsberger, A.J.P. Sabberwal, An investigation into the cutting force pulsations during milling operations, Int. J. Mach. Tool Des. Res. 1 (1966) 15–33.
[3] E. Budak, Analytical models for high performance milling, part I: cutting forces, deflections and tolerance integrity, Int. J. Mach. Tools Manuf. 46 (2006) 1478–1488.
[4] Y. Altintas, E. Budak, Analytical prediction of stability lobes in milling, Ann. CIRP 44 (1) (1995) 357–362.
[5] W.X. Tang, Q.H. Song, S.Q. Yu, S.S. Sun, B.B. Li, B. Du, X. Ai, Prediction of chatter stability in high-speed finishing end milling considering multi-mode dynamics, J. Mater. Proc. Tech. 209 (2009) 2585–2591.
[6] B.P. Mann, P.V. Bayly, M.A. Davies, J.E. Halley, Limit cycles, bifurcations, and accuracy of the milling process, J. Sound Vib. 277 (2004) 31–48.
[7] T. Insperger, G. Stepan, Updated semi-discretization method for periodic delay-differential equations with discrete delay, Int. J. Numer. Methods Eng. 61 (2004) 117–141.
[8] T. Insperger, G. Stépán, Semi-Discretization for Time-Delay Systems-Stability and Engineering Applications, Springer, New York, 2011.
[9] J. Gradisek, M. Kalveram, T. Insperger, K. Weinert, G. Stepan, E. Govekar, I. Grabec, On stability prediction for milling, J. Mach. Tools Manuf. 45 (2005) 769–781.
[10] X.H. Long, B. Balachandran, Stability analysis for milling process, J. Nonlinear Dyn 49 (2007) 349–359.
[11] Y. Ding, L.M. Zhu, X.J. Zhang, H. Ding, A full-discretization method for prediction of milling stability, Int. J. Mach. Tools Manuf. 50 (2010) 502–509.
[12] H. Moradi, F. Bakhtiari-Nejad, M.R. Movahhedy, G.R. Vossoughi, Stability improvement and regenerative chatter suppression in nonlinear milling process via tuneable vibration absorber, J. Sound Vib. 331 (21) (2012) 4668–4690.
[13] B.P. Mann, K.A. Young, T.L. Schmitz, D.N. Dilley, Simultaneous stability and surface location error predictions in milling, ASME Trans. J. Manuf. Sci. Eng. 127 (2005) 446–453.
[14] N.D. Sims, B.P. Mann, S. Huyanan, Analytical prediction of chatter stability for variable pitch and variable helix milling tools, J. Sound Vib. 317 (2008) 664–686.
[15] O.A. Bobrenkov, F.A. Khasawneh, E.A. Butcher, B.P. Mann, Analysis of milling dynamics for simultaneously engaged cutting teeth, J. Sound Vib. 329 (2010) 585–606.
[16] Y. Altintas, G. Stepan, D. Merdol, Z. Dombovari, Chatter stability of milling in frequency and discrete time domain, CIRP J. Manuf. Sci. Technol. 1 (2008) 35–44.
[17] N.D. Sims, G. Manson, B.P. Mann, Fuzzy stability analysis of regenerative chatter in milling, J. Sound Vib. 329 (2010) 1025–1041.
[18] N.H. Hanna, S.A. Tobias, A theory of nonlinear regenerative chatter, Trans. ASME J. Eng. Ind. 96 (1974) 247–255.
[19] L. Vela-Martínez, J.C. Jáuregui-Correa, O.M. González-Brambila, G. Herrera-Ruiz, A. Lozano-Guzmán, Instability conditions due to structural nonlinearities in regenerative chatter, J. Nonlinear Dyn 56 (2009) 415–427.
[20] N. Deshpande, M.S. Fofana, Nonlinear regenerative chatter in turning, J. Comput. Integ. Manuf. 17 (2001) 107–112.
[21] G. Stepan, T. Insperger, R. Szalai, Delay, parametric excitation, and the nonlinear dynamics of cutting process, Int. J. Bifurcation Chaos 15 (9) (2005) 2783–2798.
[22] F.C. Moon, T. Kalmar-Nagy, Nonlinear models for complex dynamics in cutting materials, Philos. Trans. R. Soc. London, 2001 Ser. A (1781) (2001) 695–711.
[23] H. Moradi, M.R. Movahhedy, G.R. Vossoughi, Dynamics of regenerative chatter and internal resonance in milling process with structural and cutting force nonlinearities, J. Sound Vib. 331 (16) (2012) 3844–3865.
[24] H. Moradi, M.R. Movahhedy, G.R. Vossoughi, Bifurcation analysis of milling process with tool wear and process damping: regenerative chatter with primary resonance, J. Nonlinear Dyn 70 (1) (2012) 481–509.
[25] Y.S. Tarng, J.Y. Kao, E.C. Lee, Chatter suppressions in turning operations with a tuned vibration absorber, J. Mater. Proc. Technol. 105 (2000) 55–60.
[26] H. Moradi, F. Bakhtiari-Nejad, M.R. Movahhedy, Using a vibration absorber to suppress chatter vibration in turning process with a worn tool, in: Proc. of ASME 2009 Des. Eng. Tech. Conf. & Comp. and Inf. in Eng. Conf., DETC2009-86100, California, USA, 2009.
[27] H. Moradi, F. Bakhtiari Nejad, M.R. Movahhedy, Tunable vibration absorber design to suppress vibrations: an application in boring manufacturing process, J. Sound Vib. 318 (2008) 93–108.
[28] M.H. Miguelez, L. Rubio, J.A. Loya, J. Fernandez-Saez, Improvement of chatter stability in boring operations with passive vibration absorbers, Int. J. Mech. Sci. 52 (2010) 1376–1384.
[29] K.J. Liu, K.E. Rouch, Optimal passive vibration control of cutting process stability in milling, J. Mater. Proc. Technol. 28 (1991) 285–294.
[30] A. Rashid, C.M. Nicolescu, Design and implementation of tuned viscoelastic dampers for vibration control in milling, J. Mach. Tools Manuf. 48 (2008) 1036–1053.
[31] Y.S. Liao, Y.C. Young, A new online spindle speed regulation strategy for chatter control, Int. J. Mach. Tools Manuf. 36 (5) (1996) 651–660.
[32] M. Zatarain, I. Bediaga, J. Munoa, R. Lizarralde, Stability of milling processes with continuous spindle speed variation: analysis in the frequency and time domains, and experimental correlation, CIRP Ann. – Manuf. Technol. 57 (1) (2008) 379–384.
[33] S. Seguy, T. Insperger, L. Arnaud, G. Dessein, G. Peigne, On the stability of high-speed milling with spindle speed variation, Int. J. Adv. Manuf. Technol. 48 (2010) 883–895.
[34] K.H. Hajikolaei, H. Moradi, G.R. Vossoughi, M.R. Movahhedy, Spindle speed variation and adaptive force regulation to suppress regenerative chatter in turning process, J. Manuf. Proc. 12 (2) (2010) 106–115.
[35] J.R. Pratt, A.H. Nayfeh, Chatter control and stability analysis of a cantilever boring bar under regenerative cutting conditions, Philos. Trans. R. Soc. London, Part A 359 (2001) 759–792.
[36] B.K. Fussell, K. Srinivasan, Adaptive control of force in end milling operations – an evaluation of available algorithms, J. Manuf. Syst. 10 (1) (1991) 8–20.
[37] C. Mei, Active regenerative chatter suppression during boring manufacturing process, J. Rob. Comput. Integ. Manuf. 21 (2005) 153–158.
[38] E. Abele, H. Hanselka, F. Haase, D. Schlote, A. Schiffler, Development and design of an active work piece holder driven by piezo actuators, Prod. Eng. Res. Develop. 2 (2008) 437–442.
[39] H. Moradi, M.R. Movahhedy, G.R. Vossoughi, Sliding mode control of machining chatter in the presence of tool wear and parametric uncertainties, J. Vib. Control 16 (2) (2010) 231–251.
[40] H. Moradi, M.R. Movahhedy, G.R. Vossoughi, Robust control strategy for suppression of regenerative chatter in turning, J. Manuf. Proc. 11 (2) (2009) 55–65.
[41] H. Moradi, M. Sadighi, F. Bakhtiari Nejad, Optimum design of a tunable vibration absorber with variable position to suppress vibration of a cantilever plate, Int. J. Acoust. Vib. (IJAV) 16 (2) (2011) 55–63.
[42] Y. Altintas, Manufacturing Automation: Metal Cutting Mechanics, Machine Tool Vibrations, and CNC Design, Cambridge University Press, 2000.
[43] H. Moradi, M.R. Movahhedy, G.R. Vossoughi, Linear and nonlinear model of cutting forces in peripheral milling: a comparison between 2D and 3D models, in: ASME 2010 Int. Mech. Eng. Cong. & Exp., IMECE2010-38641, British Columbia, Canada, 2010.
[44] L. Meirovitch, Principles and Techniques of Vibrations, Prentice Hall, New Jersey, 2000.
[45] A.W. Leissa, Vibration of plates, NASA SP160, US Government Printing Office, Washington, DC, 1969.
[46] T. Delio, J. Tlusty, S. Smith, Use of audio signals for chatter detection and control, Trans. ASME 114 (2) (1992) 146–157.
[47] D.A. Dornfeld, Monitoring of machining process-literature review, CIRP Ann. 41 (1) (1992) 93–96.
[48] E. Kuljanic, G. Totis, M. Sortino, Development of an intelligent multisensor chatter detection system in milling, J. Mech. Syst. Signal Proc. 23 (2009) 1704–1718.